Celestial Mechanics and Dynamical Astronomy (2021) 133:5
https://doi.org/10.1007/s10569-021-10002-2

ORIGINAL ARTICLE

Critical homoclinics in a restricted four-body problem: numerical continuation and center manifold computations

Wouter Hetebrij[1] · **J. D. Mireles James**[2]

Received: 28 July 2020 / Revised: 19 December 2020 / Accepted: 15 January 2021 /
Published online: 15 February 2021

Abstract
The present work studies the robustness of certain basic homoclinic motions in an equilateral restricted four-body problem. The problem can be viewed as a two-parameter family of conservative autonomous vector fields. The main tools are numerical continuation techniques for homoclinic and periodic orbits, as well as formal series methods for computing normal forms and center stable/unstable manifold parameterizations. After careful numerical study of a number of special cases, we formulate several conjectures about the global bifurcations of the homoclinic families.

Keywords Four-body problem · Homoclinic dynamics · Critical equilibria · Center manifold parameterization

Mathematics Subject Classification 70K44 · 34C45 · 70F15

1 Introduction

Suppose that three gravitating bodies are arranged in the equilateral triangle configuration of Lagrange. The *circular restricted four-body problem* (CRFBP) studies the dynamics of a fourth massless particle in a co-rotating reference frame. The problem was first introduced by Pedersen (1944, 1952), and we recall the equations of motion and other basic facts in Sect. 1.1. A recent work by Kepley and James (2019) studies—in the case of equal masses—certain "short" or "basic" homoclinic motions at the center of mass of the three bodies. In the present work, we are interested in the fate of these basic homoclinic motions as the system is perturbed away from the equal mass case: in particular their robustness, bifurcations, and

The first author was partially supported by NWO-VICI Grant 639033109.
The second author was partially supported by NSF Grant DMS-1813501.

✉ J. D. Mireles James
jmirelesjames@fau.edu

Wouter Hetebrij
w.a.hetebrij@vu.nl

[1] Department of Mathematics, Vrije Universiteit Amsterdam, Amsterdam, Netherlands

[2] Department of Mathematical Sciences, Florida Atlantic University, Boca Raton, USA

eventual disappearance. In preparation for this discussion, we briefly review what is known about the structure of the equilibrium set.

The equilibrium solutions—or *libration points*—of the CRFBP are the main topic of the study (Simó 1978) by Simó. In that work one finds detailed numerical evidence in support of the claim that the problem has either 8, 9, or 10 libration points, whose number and location depend on the mass ratios. This conjecture was eventually settled in the affirmative by Barros and Leandro using mathematically rigorous computer-assisted methods of proof (Leandro 2006; Barros and Leandro 2011, 2014), and we recount their results after introducing a little notation and terminology.

Appropriate choice of units results in a unit value of the gravitational constant and total mass of the system. The massive bodies are labeled according to the convention that $m_3 \leq m_2 \leq m_1$. The parameter space of the CRFBP is then reduced to the 2-simplex

$$\mathfrak{S} = \left\{(m_1, m_2, m_3) \in \mathbb{R}^3 \colon m_1 + m_2 + m_3 = 1, \text{and} m_3 \leq m_2 \leq m_1\right\},$$

determined by the vertices $v_0 = (1/3, 1/3, 1/3)$, $v_1 = (1/2, 1/2, 0)$, and $v_2 = (1, 0, 0)$.

We refer to the special system with mass parameters $m_1 = m_2 = m_3 = 1/3$ as the *triple Copenhagen problem*. This is a nod to the traditional name of the equal mass case of the circular restricted three-body problem (CRTBP), which is called *the Copenhagen problem* in honor of the work done at the Copenhagen observatory in the first decades of the twentieth century during the tenure of Elis Strömgren. See, for example, the review article (Strömgren 1934) by Strömgren, as well as the detailed discussion in Chapter 9 of the book of Szebehely (1967).

We remark that if $m_3 = 0$, then the CRFBP reduces to the CRTBP, and that if $m_2 = m_3 = 0$, then the problem reduces further to the rotating Kepler problem. The CRTBP is treated in great detail elsewhere, and we will not dwell on it further other than to say that the problem is well known to have five libration points for all values of the mass ratio $\mu = m_2/m_1 \neq 0$. For much more thorough discussion, we refer the interested reader again to Chapter 9 of the book of Szebehely (1967), or to the more modern treatment in the book of Meyer and Offin (2017).

We refer to an equilibrium solution in the interior of the closed equilateral triangle as an *inner libration point*, and an equilibrium in the complement of this triangle as an *outer libration point*. A schematic illustrating the phase space is given in Fig. 2. From Leandro (2006), Barros and Leandro (2011), Barros and Leandro (2014) we have the following complete description of the equilibrium set:

- (I) For each $(m_1, m_2, m_3) \in \mathfrak{S}$ with $m_3 > 0$, there are six outer libration points. We denote these by $L_{4,5,6,7,8,9}$.
- (II) There is an analytic, simple closed curve $\mathfrak{D} \subset \mathfrak{S}$ from the $m_1 = m_2$ edge to the $m_2 = m_3$ edge of the simplex. The number of libration points is constant throughout $\mathfrak{S}$, except on $\mathfrak{D}$. We refer to $\mathfrak{D}$ as the *critical parameter curve*. $\mathfrak{D}$ does not contain any vertex, nor does it intersect the $m_3 = 0$ edge of the simplex.
- (IV) $\mathfrak{S}\backslash\mathfrak{D}$ has two components which we denote by $\mathfrak{S}_I$ and $\mathfrak{S}_{II}$. We take $\mathfrak{S}_I$ to be the component containing the triple Copenhagen vertex v_0. For each $(m_1, m_2, m_3) \in \mathfrak{S}_I$, the system has 4 inner libration points, making ten in total. For each $(m_1, m_2, m_3) \in \mathfrak{S}_{II}$ with $m_3 > 0$, the system has 2 inner libration points, making 8 total.
- (V) If $(m_1, m_2, m_3) \in \mathfrak{D}$ and $m_1 \neq m_2$, then the system has 3 inner libration points, making for 9 total. Denote by $v_{\text{pf}} \in \mathfrak{S}$ the point where $\mathfrak{D}$ intersects the $m_1 = m_2$ edge (the reason for the "pf" will be made clear below). When the system has parameters v_{pf}, there are 2 inner libration points, for a total of 8.

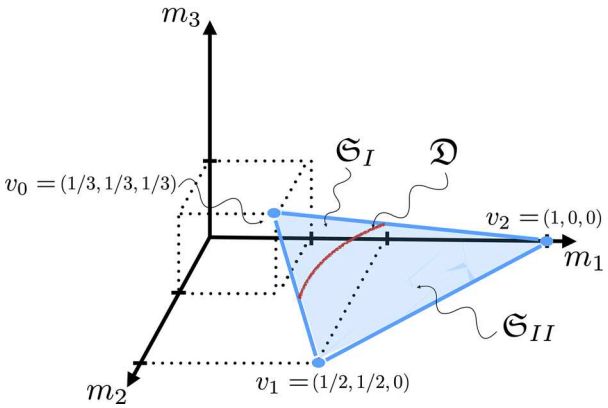

Fig. 1 Parameter simplex for the CRFBP: normalizing so that $m_1 + m_2 + m_3 = 1$ with $m_3 \leq m_2 \leq m_1$ leads to a parameter space as depicted in the figure. The simplex is formed by the vertices $v_0 = (1/3, 1/3, 1/3)$ corresponding to equal masses (triple Copenhagen problem), $v_1 = (1/2, 1/2, 0)$ corresponding to all mass in two equal primaries (restricted three-body Copenhagen problem), and $v_2 = (1, 0, 0)$ where all the mass is in the largest body (rotating Kepler problem). Observe that $m_2 = m_3$ along the edge joining v_0 and v_2, that $m_1 = m_2$ along the edge joining v_0 and v_1, and that $m_3 = 0$ along the edge joining v_1 and v_2. The critical parameter curve $\mathfrak{D}$ is depicted as a red arc from the $m_1 = m_2$ edge to the $m_2 = m_3$ edge, cutting the simplex in two components denoted $\mathfrak{S}_I$ and $\mathfrak{S}_{II}$. In $\mathfrak{S}_I$, the system has ten equilibrium solutions and in $\mathfrak{S}_{II}$ only eight. The number changes only on the critical curve $\mathfrak{D}$ where the inner libration point L_0 loses hyperbolicity and annihilates with L_2. See Fig. 2 for the approximate locations of the $8 - 10$ libration points

The parameter simplex is illustrated schematically in Fig. 1.

Let us elaborate on statements (IV) and (V). With $(m_1, m_2, m_3) \in \mathfrak{S}_I$, denote the 4 inner libration points by $L_{0,1,2,3}$ (as in Fig. 2). Since there are no bifurcations in $\mathfrak{S}_I$, the locations of the libration points vary continuously (even analytically) throughout this region. In the triple Copenhagen problem, the libration point L_0 is located at the center of mass/origin in state space. For all parameters in $\mathfrak{S}_I$, L_0 has saddle type stability (two stable and two unstable eigenvalues) and the libration points $L_{1,2,3}$ have saddle $\times$ centers stability (one stable, one unstable and a pair of purely imaginary conjugate eigenvalues).

Suppose that parameters are varied continuously from a point in the region $\mathfrak{S}_I$ to a point in the region $\mathfrak{S}_{II}$. As the parameters cross the critical curve $\mathfrak{D}$, the system undergoes a bifurcation involving L_0 and L_2. In the general case that $m_1 \neq m_2$, the bifurcation is a Hamiltonian saddle node wherein L_0 and L_2 collide and annihilate. At v_{pf}—where $\mathfrak{D}$ intersects the $m_1 = m_2$ edge—the bifurcation is a Hamiltonian pitchfork bifurcation involving L_0, L_2, and L_3. Again, L_0 and L_2 vanish in this pitchfork bifurcation so that in every case it is only the inner libration points L_1 and L_3 which remain once $(m_1, m_2, m_3) \in \mathfrak{S}_{II}$. We write L_{sn} to denote the libration point at saddle node bifurcation, and L_{pf} for the pitchfork. We sometimes write L_c to denote a critical libration point without specifying whether we are at the pitchfork or a saddle node bifurcation.

Given that the equilibrium structure of the CRFBP is completely understood, one natural line of inquiry is to study orbits homoclinic to the equilibria, and any possible bifurcations of these homoclinic connecting orbits. For example, bifurcations at L_0 when the system crosses the critical curve $\mathfrak{D}$ must trigger corresponding bifurcations for orbits homoclinic to L_0. Some studies which consider heteroclinic and homoclinic connections in the CRFBP are Burgos-García and Delgado (2013), and Baltagiannis and Papadakis (2011). The present

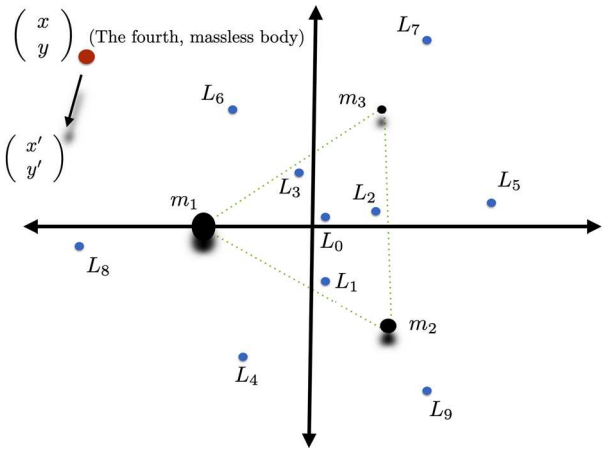

Fig. 2 Configuration space for the CRFBP: The three primary bodies with masses m_1, m_2, and m_3 are arranged in an equilateral triangle configuration of Lagrange, which is a relative equilibrium solution of the three-body problem. After transforming to a co-rotating frame, we consider the motion of a fourth massless body. The equations of motion have 8, 9, or 10 equilibrium solutions (libration points) denoted by L_j for $0 \leq j \leq 9$. The number of libration points and their stability vary depending on m_1, m_2, and m_3. The points $L_{0,4,5,6}$ have saddle focus stability for some values of the masses. The other libration points have either saddle $\times$ center or center $\times$ center stability type for all values of the masses

work builds on the recent study of homoclinic phenomena in the triple Copenhagen problem by Kepley and James (2019).

Relevant results from Kepley and James (2019) are reviewed in Sect. 1.3. What is important for the purposes of the present introduction is that there are six basic homoclinic motions at triple Copenhagen L_0, denoted by $\gamma_{1,2,3,4,5,6} \colon \mathbb{R} \to \mathbb{R}^4$ (see Fig. 4), and that these basic connections appear to organize all observed homoclinic phenomena at L_0. Given the importance of $\gamma_{1,2,3,4,5,6}$ in the triple Copenhagen problem, it is natural to investigate their role as parameters vary. This leads to some fairly delicate questions about the global dynamics. The present work focuses primarily on the "shortest" homoclinics $\gamma_{1,2,3}$.

- *Question 1* The connections $\gamma_{1,2,3}$ are transverse (in the Hamiltonian sense), and hence persist for parameter values $(m_1, m_2, m_3) \approx v_0$. *What happens to* $\gamma_{1,2,3}$ *as the mass parameters move throughout* $\mathfrak{S}_1$ *toward* $\mathfrak{D}$*?* In particular, how robust are the connections? Do any of the connections survive all the way to $\mathfrak{D}$?
- *Question 2* With $(m_1, m_2, m_3) \in \mathfrak{D}$ consider the critical libration point L_c. *Are there homoclinic connections to the critical libration point?* How are they related to the basic homoclinic motions $\gamma_{1,2,3}$ of the triple Copenhagen problem?

The CRFBP has a conserved, energy-like quantity known as the Jacobi integral (see Sect. 1.1). Systems with first integrals enjoy an intimate relationship between homoclinic orbits and one parameter families of periodic orbits. This connection was first studied by Strömgren in connection with the (CRTBP) (see, for example, (Strömgren 1934)) where it was observed that some planar families of Lyapunov periodic orbits appear to accumulate to "asymptotic periodic orbits"—heteroclinic cycles or homoclinic orbits in modern terminology. This phenomenon involves a global bifurcation made precise by the "blue sky catastrophe" of Henrard (1973), Devaney (1977), Burgos-García and Delgado (2013), Shilnikov et al. (2014).

It was observed in Kepley and James (2019) that each of the short homoclinics $\gamma_{1,2,3}$ participates in a blue sky catastrophe, appearing as the limit of the planar Lyapunov family associated with the inner libration it winds around. More precisely, the planar family of periodic orbits attached to L_i accumulates to γ_i, for $i = 1, 2, 3$. This leads to a third question concerning the phase space structure of the CRFBP at criticality.

– *Question 3* For $(m_1, m_2, m_3) \in \mathfrak{D}$, What is the asymptotic fate of the planar Lyapunov families attached to L_1 and L_3? Do these families participate in blue sky castrophies with critical homoclinic orbits at L_c? If not, where do they accumulate? (Recall that L_2 has collided with L_0 on the critical curve, so that question only makes sense for $L_{1,3}$.)

These three questions are the main topic of the present study, and are addressed using tools from computational dynamics. In particular, we apply numerical continuation methods for periodic/homoclinic orbits, as well as high-order numerical methods for computing invariant manifolds attached to libration points. These topics are standard and have been discussed at length in other places, and we provide some references when appropriate below. We include, for the sake of completeness, a short overview of numerical continuation schemes in conservative system as Appendix A. We also employ high-order methods for computing center and center stable/unstable manifolds, as well as normal form calculations, to illuminate the dynamics at $\mathfrak{D}$. We will see that the three questions are interrelated, so that understanding any one of them provides information about the other two.

More precisely, we are guided by the following qualitative observations, whose judicious use leads to quantitate information about bifurcations of the homoclinics orbits. For numerical continuations, we will always consider parameter curves starting at v_0 and terminating at the critical curve $\mathfrak{D}$. This leads to one parameter continuation problems, so that bifurcations then occur at isolated parameter points, and we can talk about what happens before and after such a bifurcation point.

– *Approximating bifurcation parameters from below—robustness of numerical continuation* suppose that we vary the mass parameters of the system from v_0 toward the critical curve $\mathcal{D}$, and apply a numerical continuation scheme to one of the homoclinic orbits $\gamma_{1,2,3}$. Then, a breakdown in the numerical continuation scheme indicates a possible bifurcation of the homoclinic family. Breakdown is indicated by the loss of invertibility (or poor numerical conditioning) of a certain matrix. The numerical scheme will breakdown before the bifurcation so that the blow up of the condition number provides a useful lower bound on the approximate location of the bifurcation parameter. This is the topic of Sect. 2.
– *Approximating bifurcation parameters from above—the blue sky test* as mentioned above, the "tubes" of planar Lyapunov periodic orbits originating at $L_{1,2,3}$ in the triple Copenhagen problem accumulate to the interior homoclinic orbits $\gamma_{1,2,3}$. This phenomena is robust, and hence persists for small changes in parameters. Then, studying the limiting behavior of a Lyapunov tube provides another qualitative feature that can only change at a bifurcation of the homoclinic orbit. Numerically locating a Lyapunov tube which no longer accumulates to $\gamma_{1,2,3}$ suggests that we have passed a bifurcation of the homoclinic, and provides a useful geometric mechanism for obtaining upper bounds on the bifurcation parameter. This is the topic of Sect. 3.
– *Bifurcations on the critical curve—normal form calculations:* in some cases the continuation robustness and/or blue sky tests are inconclusive. In particular, the tests have a difficult time distinguishing bifurcations which occur near, but not on, the critical curve $\mathcal{D}$. In this case, it is helpful to examine the normal form at the critical equilibrium solution L_c, as it provides local information about connecting orbits. It can also be useful to

numerically study intersections of the center stable/center unstable manifolds in the L_c level set of the Jacobi integral. This is the topic of Sect. 4.

Using these numerical techniques in concert provides a novel approach to the qualitative study of global continuation and bifurcation properties of connecting orbits in conservative systems.

The remainder of the paper is organized as follows: In sects. 1.1 to 1.4, we review the equations of motion, a numerical method for computing critical equilibria/parameter sets, results about homoclinic motions in the triple Copenhagen problem, as well as the literature on homoclinic bifurcations. In Sect. 2, we study the $\gamma_{1,2,3}$ families via numerical continuation algorithms, while Sect. 3 is devoted to blue sky catastrophes. In Sect. 4, we study the dynamics on $\mathfrak{D}$ using numerically computed center stable/unstable manifolds and normal forms. Our conclusions are summarized in Sect. 5, and Appendices A and B provide details on multiple shooting/continuation schemes and computing the center as well as center stable/unstable manifolds.

1.1 CRFBP: equations of motion and basic properties

Define

$$K = m_2(m_3 - m_2) + m_1(m_2 + 2m_3).$$

The locations (x_1, y_1), (x_2, y_2) and (x_3, y_3) of the three primary bodies are given by

$$x_1 = \frac{-|K|\sqrt{m_2^2 + m_2m_3 + m_3^2}}{K}, \qquad y_1 = 0,$$

$$x_2 = \frac{|K|\left[(m_2 - m_3)m_3 + m_1(2m_2 + m_3)\right]}{2K\sqrt{m_2^2 + m_2m_3 + m_3^2}}, \qquad y_2 = \frac{-\sqrt{3}m_3}{2m_2^{3/2}}\sqrt{\frac{m_2^3}{m_2^2 + m_2m_3 + m_3^2}},$$

$$x_3 = \frac{|K|}{2\sqrt{m_2^2 + m_2m_3 + m_3^2}}, \qquad y_3 = \frac{\sqrt{3}}{2\sqrt{m_2}}\sqrt{\frac{m_2^3}{m_2^2 + m_2m_3 + m_3^2}}.$$

Let

$$\Omega(x, y) \overset{\text{def}}{=} \frac{1}{2}(x^2 + y^2) + \frac{m_1}{r_1(x, y)} + \frac{m_2}{r_2(x, y)} + \frac{m_3}{r_3(x, y)}, \tag{1}$$

where

$$r_j(x, y) \overset{\text{def}}{=} \sqrt{(x - x_j)^2 + (y - y_j)^2}, \qquad j = 1, 2, 3, \tag{2}$$

and write $\mathbf{x} = (x, \dot{x}, y, \dot{y}) \in \mathbb{R}^4$ to denote the state of the system. The equations of motion in the co-rotating frame are given by

$$\mathbf{x}' = f(\mathbf{x}),$$

where

$$f(x, \dot{x}, y, \dot{y}) \overset{\text{def}}{=} \begin{pmatrix} \dot{x} \\ 2\dot{y} + \frac{\partial \Omega}{\partial x} \\ \dot{y} \\ -2\dot{x} + \frac{\partial \Omega}{\partial y} \end{pmatrix}. \tag{3}$$

Observe that Ω and hence f depend in a complicated way on the masses m_1, m_2, m_3 through the positions (x_i, y_i), $i = 1, 2, 3$ of the primaries.

The system conserves the *Jacobi integral*

$$E(x, \dot{x}, y, \dot{y}) = -\left(\dot{x}^2 + \dot{y}^2\right) + 2\Omega(x, y). \tag{4}$$

Assuming that $(m_1, m_2, m_3) \in \mathfrak{S}_I$, the libration points (equilibrium solutions of Eq. (3)) are arranged as illustrated in the schematic of Fig. 2. If $(m_1, m_2, m_3) \in \mathfrak{S}_{II}$, then the equilibrium solutions are as in the schematic, except that L_0 and L_2 are not present.

There is a substantial literature on the CRFBP, and in addition to the references cited above, we refer the interested reader also to the works of Baltagiannis and Papadakis (2011), and Álvarez-Ramírez and Vidal (2009) where many of the systems basic properties are discussed in detail. Elementary families of periodic orbits are considered by Papadakis in Papadakis (2016a, b), and by Burgos–García, Bengochea, and Delgado in Burgos-García and Delgado (2013), Burgos-Garcia and Bengochea (2017). A study by Burgos-García, Lessard, and Mireles James proves the existence of a number of spatial periodic orbits for the CRFBP (Burgos-García et al. 2018) (again with computer assistance). An associated Hill's problem is derived, and its periodic orbits are studied by Burgos-García and Gidea in Burgos-García (2016); Burgos-García and Gidea (2015). Murray and Mireles James study transverse homoclinic chaos in the spatial CRFBP, for certain vertical Lyapunov families of periodic orbits attached to the inner and outer libration points (Murray and James 2020).

Regularization of collisions is studied by Álvarez–Ramírez, Delgado, and Vidal in Alvarez-Ramírez et al. (2014). Chaotic motions were studied numerically by Gidea and Burgos in Gidea and Burgos (2003), and by Álvarez–Ramírez and Barrabés in Alvarez-Ramírez and Barrabés (2015). Perturbative proofs of the existence of chaotic motions are found in the work of Cheng and She (2017), She and Cheng (2014), She et al. (2013), and also in the work of Alvarez-Ramírez et al. (2018). A computer-assisted method of proof for establishing the existence of chaotic motions at non-perturbative parameter values was developed by Kepley and Mireles James in Kepley and James (2019).

1.2 Equilibria: the critical case

In the following discussion we treat m_1, m_2 as free parameters, eliminating the parameter m_3 via the equation $m_3 = 1 - m_1 - m_2$. To characterize the critical curve we seek values of m_1 and m_2 such that Df is non-invertible at one of its Lagrangian points. The following proposition tells us in terms of the second derivatives of Ω whether or not Df is invertible, and is used to (numerically) compute the bifurcation curve $\mathfrak{D}$. We also recover that a critical libration point always has a double zero eigenvalue. See Fig. 3.

Proposition 1 (Bifurcation value) *The linearization of f at a libration point $L = (x_0, 0, y_0, 0)$ has an eigenvalue 0 iff $\Omega_{xx}(x_0, y_0)\Omega_{yy}(x_0, y_0) = \Omega_{xy}^2(x_0, y_0)$. In particular,*

- *If L_c is a critical libration point for the CRFBP, then $Df(L_c)$ has eigenvalue 0 with algebraic multiplicity 2 and geometric multiplicity 1.*

The eigenvector and generalized eigenvector corresponding to the eigenvalue 0 are

$$\mathbf{v}_0 \overset{\text{def}}{=} (\Omega_{yy}(x_0, y_0), 0, -\Omega_{xy}(x_0, y_0), 0),$$
$$\mathbf{v}_1 \overset{\text{def}}{=} (\Omega_{xy}(x_0, y_0), \Omega_{yy}(x_0, y_0), 2 - \Omega_{xx}(x_0, y_0), -\Omega_{xy}(x_0, y_0)).$$

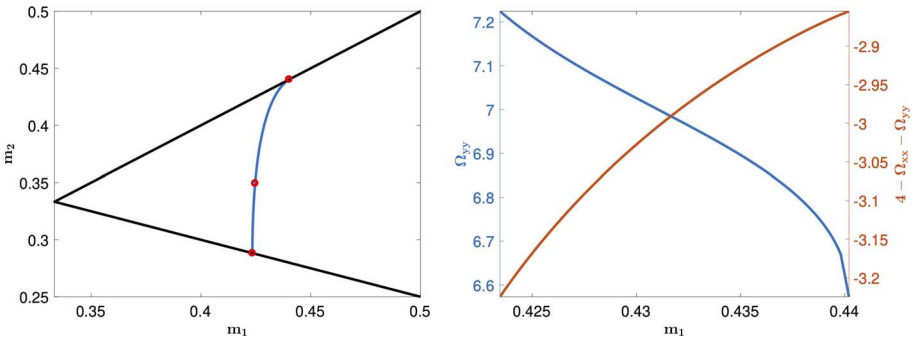

Fig. 3 Critical equilibria: left frame—parameter simplex projected into the m_1, m_2 plane. The blue curve is the numerically computed critical arc $\mathfrak{D}$. The red dots denote special critical system parameters considered throughout this work. The lower red dot depicts the intersection of $\mathfrak{D}$ with the $m_2 = m_3$ edge of the simplex. The upper red dot the intersection of $\mathfrak{D}$ with the $m_1 = m_2$ edge. The middle red dot is an arbitrarily chosen parameter set on $\mathfrak{D}$ interior to $\mathfrak{S}$. Right frame—the functions Ω_{yy} and $4 - \Omega_{xx} - \Omega_{yy}$ for the critical libration point L_c on $\mathfrak{D}$

We start with a preliminary claim:

Claim Let $\mathbf{x}_0 = (x_0, 0, y_0, 0)$ be a libration point of f. If $\Omega_{xx}(x_0, y_0)\Omega_{yy}(x_0, y_0) = \Omega_{xy}^2(x_0, y_0)$, then both $\Omega_{yy}(x_0, y_0)$ and $4 - \Omega_{xx}(x_0, y_0) - \Omega_{yy}(x_0, y_0)$ are nonzero.

Convincing evidence for the claim is obtained by computing the Critical curve as illustrated in Fig. 3. One then plots $\Omega_{yy}(x_0, y_0)$ and $4 - \Omega_{xx}(x_0, y_0) - \Omega_{yy}(x_0, y_0)$ for all (x_0, y_0) in the critical curve and checks that they are numerically indeed far from zero. A complete proof follows from the results of Leandro (2006), Barros and Leandro (2011), Barros and Leandro (2014).

Proof of Proposition 1 Writing $\Omega_{xx} = \Omega_{xx}(x_0, y_0)$, $\Omega_{yy} = \Omega_{yy}(x_0, y_0)$, and $\Omega_{xy} = \Omega_{xy}(x_0, y_0)$, we have

$$p_{Df(L)}(\lambda) \overset{\text{def}}{=} \begin{vmatrix} -\lambda & 1 & 0 & 0 \\ \Omega_{xx} & -\lambda & \Omega_{xy} & 2 \\ 0 & 0 & -\lambda & 1 \\ \Omega_{xy} & -2 & \Omega_{yy} & -\lambda \end{vmatrix} = \lambda^4 + \left(4 - \Omega_{xx} - \Omega_{yy}\right)\lambda^2 + \Omega_{xx}\Omega_{yy} - \Omega_{xy}^2. \quad (5)$$

Then, $Df(L)$ has an eigenvalue 0 iff $\Omega_{xx}\Omega_{yy} = \Omega_{xy}^2$. From our claim it follows that 0 is a double root as $\Omega_{xx} + \Omega_{yy} \neq 4$. Furthermore, from the same claim it also follows that $\Omega_{yy} \neq 0$ and hence $\mathbf{v}_0 \neq \mathbf{0}$. Direct calculation shows $Df(\mathbf{x}_0)\mathbf{v}_0 = \mathbf{0}$ and $Df(\mathbf{x}_0)\mathbf{v}_1 = \mathbf{v}_0$. □

In Introduction, we claimed that at v_{pf} there is a Hamiltonian pitchfork bifurcation instead of a Hamiltonian saddle node bifurcation. That is, we claim that the following bifurcations occur on $\mathfrak{D}$.

Claim Let $v_c = (m_1, m_2, m_3) \in \mathfrak{D}$ be a critical parameter set.

- If $m_1 \neq m_2$, the libration points L_0 and L_2 undergo a Hamiltonian saddle node bifurcation.
- If $m_1 = m_2$, the libration points L_0, L_2 and L_3 undergo a Hamiltonian pitchfork bifurcation.

We sketch the proof of this claim. First, we note that depending on the symmetries of the problem, both the Hamiltonian saddle node bifurcations and the Hamiltonian pitchfork bifurcation are co-dimension one. So, for example, one would assume that for $v \in \mathfrak{D}$ with neither $m_1 = m_2$ nor $m_2 = m_3$ the bifurcation at v is a saddle node bifurcation thanks to lack of symmetry. Furthermore, as we will see in Lemma B.2, if the constant

$$\Omega_{xxx}\Omega_{yy}^3 - 3\Omega_{xxy}\Omega_{yy}^2\Omega_{xy} + 3\Omega_{xyy}\Omega_{yy}\Omega_{xy}^2 - \Omega_{yyy}\Omega_{xy}^3 \neq 0,$$

at the critical libration point L_c, then the dynamics near the critical libration point resembles Fig. 17. We will show numerically that for $v_c = (m_1, m_2, m_3) \in \mathfrak{D}$ with $m_1 \neq m_2$, we have

$$\Omega_{xxx}\Omega_{yy}^3 - 3\Omega_{xxy}\Omega_{yy}^2\Omega_{xy} + 3\Omega_{xyy}\Omega_{yy}\Omega_{xy}^2 - \Omega_{yyy}\Omega_{xy}^3 < 0,$$

supporting the first part of the claim.

Moreover, in Sect. 4 we compute the normal form for $v_c = (m_1, m_2, m_3) \in \mathfrak{D}$ at the left end point of $\mathfrak{D}$. That is, at the intersection of $\mathfrak{D}$ with the $m_2 = m_3$ edge. We then compute the normal form for $v_c = (m_1, m_2, m_3) \in \mathfrak{D}$ when $m_1 = 0.4247$, a "generic point" in $\mathfrak{D}$. In both cases, we find that the vector field on the center manifold agrees numerically with the normal form of the saddle node bifurcation. This provides even further support for the first claim.

For the second part of the claim, we analytically show that

$$\Omega_{xxx}\Omega_{yy}^3 - 3\Omega_{xxy}\Omega_{yy}^2\Omega_{xy} + 3\Omega_{xyy}\Omega_{yy}\Omega_{xy}^2 - \Omega_{yyy}\Omega_{xy}^3 = 0$$

at the libration point L_c for $v_{\text{pf}} \in \mathfrak{D}$. Furthermore, in Sect. 4, we will also compute the vector field on the center manifold for $v_{\text{pf}} \in \mathfrak{D}$ which agrees numerically with the normal form of the pitchfork bifurcation, supporting the second part of the claim.

1.3 Short homoclinic connections in the triple Copenhagen problems

Homoclinic connecting orbits for the saddle-focus equilibria in the triple Copenhagen problem were studied in detail in Kepley and James (2019). The main result at L_0 is that there are six basic homoclinic orbits which appear to organize the full web of connections. These are denoted $\gamma_i : \mathbb{R} \to \mathbb{R}^4$ for $i = 1, \ldots, 6$ and are illustrated in Fig. 4. These orbits are the shortest homoclinics, both in terms of arc length and time of flight from a local unstable to a local stable invariant manifold. The shortest orbits $\gamma_1, \gamma_2, \gamma_3$ each wind once around the libration point L_1, L_2 or L_3, respectively. Indeed, each appears to participate in a blue sky catastrophe with the corresponding planar Lyapunov family.

There appear to be infinitely many additional homoclinic orbits "shadowing" the basic connections in any order we wish. That is, consider a word Γ composed of any combination of the letters γ_i, $i = 1, \ldots, 6$. There is a homoclinic orbits which passes close to γ_i in the prescribed order. These results and more are discussed in detail in Kepley and James (2019).

An important remark is that the results of Kepley and James (2019) show numerically that the homoclinics γ_i, $i = 1, \ldots, 6$ are transverse in the energy level set of L_0. Then, each of the homoclinic orbits persist for a small change in parameter values. While some preliminary numerical continuations were discussed in Kepley and James (2019), the calculations were neither systematic nor were they take all the way to the critical curve $\mathfrak{D}$.

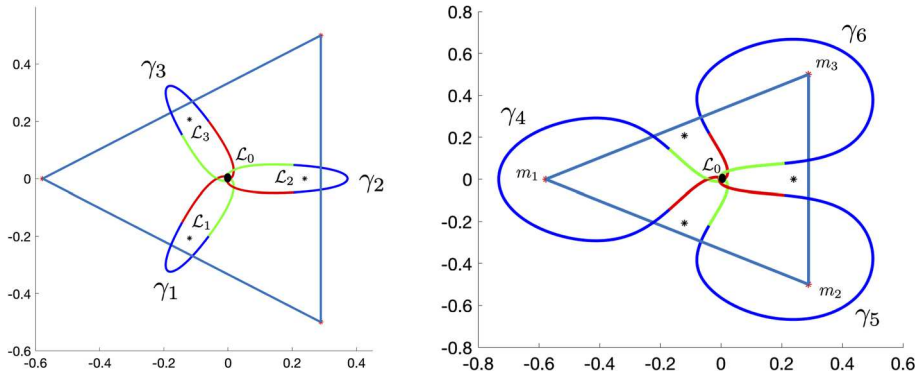

Fig. 4 Fundamental homoclinics at L_0**:** Left frame—the three shortest homoclinic orbits at L_0, which we refer to as $\gamma_{1,2,3}$ depending on which libration point they wind around. Right frame—the fourth, fifth, and sixth shortest homoclinics at L_0, which we refer to as $\gamma_{4,5,6}$. In the triple Copenhagen problem these orbits are related by rotational symmetry; however, continuation away from equal masses will break this symmetry. In both frames the red and green part of the homoclinic is the portion described by the parameterized local unstable and stable manifolds, respectively. The blue portion of the curve is obtained by solving the projected boundary value problem

1.4 Hamiltonian homoclinic bifurcations: classic results

Homoclinic orbits are fundamental objects of study in dynamical systems theory, and there exists a vast literature on their properties, numerical calculation, and bifurcations. Even in the special case of Hamiltonian systems, this is a rich area and we only recall as much of the theory as pertains directly to the present study. A fantastic overview of this theory with an in-depth discussion of the literature is found in Champneys (1998). We identify five types of global bifurcations involving homoclinic connections in Hamiltonian systems. We state the results for four-dimensional vector fields, though more general results are found in the references.

- *Type I—Hamiltonian bi-focus homoclinics* Suppose that $f : \mathbb{R}^4 \to \mathbb{R}^4$ is a Hamiltonian vector field and that $L \in \mathbb{R}^4$ is an equilibrium solution with complex conjugate eigenvalues $\pm\alpha \pm i\beta$, $\alpha, \beta > 0$. Assume that $\gamma : \mathbb{R} \to \mathbb{R}^4$ is a transverse homoclinic orbit for L. Then, there are infinitely many chaotic horseshoes near γ. See Devaney (1976). In addition, there is a tube of periodic orbits accumulating to γ. See Henrard (1973), Shilnikov et al. (2014). This is the "blue sky" catastrophe already mentioned above.
- *Type II—Belyakov–Devaney bifurcation* Suppose that $f(x, \mu)$ is a one-parameter family of Hamiltonian systems, and that for $\mu \in (\mu_0 - \epsilon, \mu_0 + \epsilon)$, $L(\mu)$ is a libration point for the vector field $f(x, \mu)$. Suppose that for $\mu < \mu_0$ $L(\mu)$ is a bi-focus, and that for $\mu > \mu_0$ $L(\mu)$ has real distinct eigenvalues $\pm\alpha, \pm\beta$, $\alpha, \beta > 0$. Then, $L(\mu_0)$ has real repeated eigenvalues. Assume that the repeated eigenvalues have geometric multiplicity one, and algebraic multiplicity two, and that $\gamma_\mu(t)$ is a smooth family of homoclinic connecting orbits for $L(\mu)$. Then, (under some generic non-degeneracy assumptions) there are infinitely many homoclinic doubling bifurcations of $\gamma_{\mu_0}(t)$ at μ_0. For the precise statement of the theorem and its proof see Champneys and Toland (1993).
- *Type III—Transverse connections to a Hamiltonian saddle node* Suppose that $f(x, \mu)$ is a one-parameter family of Hamiltonian systems with a saddle-node bifurcation at μ_0. To be more precise, let $L \in \mathbb{R}^4$ denote the critical libration point and suppose that L

has a double zero eigenvalue with geometric multiplicity one, algebraic multiplicity two, and two real eigenvalues $\pm\alpha$. Moreover, the normal form at L has nonzero quadratic term. Then, L has three-dimensional center stable and three-dimensional center unstable manifolds. The restriction of these three-dimensional center stable/unstable manifolds to the energy level set of L results in a pair of two dimensional invariant manifolds, which may intersect transversally in the energy level, giving rise to a non-degenerate homoclinic orbit γ. In general, there will be two families of transverse homoclinic orbits which annihilate at γ, and a family of periodic orbits born out of the disappearance of γ. The precise statement of the theorem and its proof are found in Weihua and Huang (2003).

- *Type IV—Degenerate homoclinic orbits in conservative systems* this co-dimension one phenomenon is studied in Knobloch (1997), Homburg and Knobloch (2005). A transverse homoclinic orbit in a one-parameter family of Hamiltonian systems can be continued until the loss of transversality. In short, the theorem states that before the bifurcation the generic situation is that there is a pair of transverse homoclinic orbits which collide and annihilate at criticality. After the bifurcation the homoclinic families are gone.
- *Type V—Degenerate connection to a Hamiltonian saddle node* In a two-parameter Hamiltonian system a type III homoclinic bifurcation can be continued along a one-dimensional curve in parameter space until the critical homoclinic loses transversality. In short, the result is that near a non-transverse critical homoclinic orbit there is a pair of critical transverse homoclinic orbits which collide and annihilate. See Deng (1990), Champneys et al. (1996) for more complete discussion.

In addition, near a Hamiltonian saddle-node or Hamiltonian pitchfork bifurcation, normal form analysis provides additional local homoclinic bifurcations. For example, near a Hamiltonian saddle node bifurcation there are two families of libration points $L_1(\mu)$ and $L_2(\mu)$ which collide and annihilate at μ_0. Without loss of generality, we have that $L_1(\mu)$ has distinct real eigenvalues and $L_2(\mu)$ has saddle-center stability for $\mu < \mu_0$. Analysis of the normal form shows that there is a family of "small" homoclinic orbits for $L_1(\mu)$, which wind around $L_2(\mu)$ for $\mu < \mu_0$. This family of homoclinic orbits shrink and disappear when $L_1(\mu)$ and $L_2(\mu)$ collide and annihilate at μ_0. See, for example, Iooss and Kirchgässner (1992), Broer et al. (1995). Near a Hamiltonian pitch fork a similar normal form analysis shows that near the pitch fork there are two families (related by symmetry) of "small" homoclinic orbits which disappear in the pitch fork bifurcation. See again Iooss and Kirchgässner (1992), Broer et al. (1995).

These classical results inform our intuition throughout the remainder of the paper.

2 Robustness of the short Copenhagen L_0 homoclinics

We now consider robustness with respect to parameter perturbations of γ_j for $j = 1, 2, 3$. Our idea is to use classical numerical continuation algorithms for Hamiltonian homoclinic connections to study the γ_j as the parameters of the system are moved away from $v_0 = (1/3, 1/3, 1/3)$. Numerical continuation algorithms for periodic and connecting orbits are reviewed briefly in Appendix A for the sake of completeness; however, the reader seeking a thorough overview is referred to the classic works of Doedel and Friedman (1989), Muñoz Almaraz et al. (2003), Doedel et al. (2003), Calleja et al. (2012).

We fix three lines in parameter space, each starting at v_0 and terminating on $\mathfrak{D}$ so that we obtain three one-parameter continuation problems. To begin, we numerically compute three

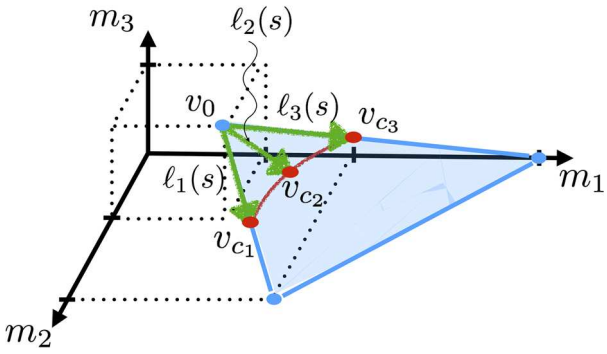

Fig. 5 Three parameter continuation arcs: consider three critical parameter sets v_{c_1}, v_{c_2}, and v_{c_3} on the curve $\mathfrak{D}$ and define the lines from v_0 to each of these. We denote the lines by $\ell_1(s)$, $\ell_2(s)$, and $\ell_3(s)$, and study the one-parameter numerical continuation problem for γ_1, γ_2, and γ_3 on these lines

critical parameter sets $v_{c_1}, v_{c_2}, v_{c_3} \in \mathfrak{D}$ with

$$v_{c_1} \approx \begin{pmatrix} 0.440201606048930 \\ 0.440201606048930 \\ 0.119596787902140 \end{pmatrix}, \quad v_{c_2} \approx \begin{pmatrix} 0.4247 \\ 0.349370273506504 \\ 0.225929726493496 \end{pmatrix}, \quad \text{and}$$

$$v_{c_3} \approx \begin{pmatrix} 0.423447616433011 \\ 0.288276191783495 \\ 0.288276191783495 \end{pmatrix}.$$

Here v_{c_1} is on the $m_1 = m_2$, and v_{c_3} on the $m_2 = m_3$ parameter edges, respectively. The parameters v_{c_2} are taken near "the middle" of the critical curve, with $m_1 = 0.4247$ fixed somewhat arbitrarily. Define the parameter lines

$$\ell_k(s) = (1-s)v_0 + sv_{c_k},$$

where $k = 1, 2, 3$. The critical parameters and parameter curves are illustrated schematically in Fig. 5.

Since the homoclinic orbits γ_j for $j = 1, 2, 3$ are transverse in the L_0 energy level set of the triple Copenhagen problem, each persists under small changes in the parameters. We write $\gamma_{j,k}(s)$ to denote the one-parameter family of homoclinic orbits obtained by parameter continuation of γ_j along the parameter line $\ell_k(s)$. Following the discussion in Sect. 1.4, a homoclinic connection can breakdown/disappear only under one of the two following scenarios:

- (A) loss of transversality, or
- (B) disappearance of the underlying equilibrium solution itself.

Note that in scenario (A) the equilibrium solution may persist after the homoclinic disappears, and that scenario (B) occurs only at $\mathfrak{D}$. So for a given $1 \leq j, k \leq 3$, the question is: *does that family $\gamma_{j,k}(s)$ survive all the way to $\mathfrak{D}$ or does it breakdown before?*

The question is made more quantitative as follows: Since transversality is an open condition, there exist $0 < \hat{s}_{j,k} \leq 1$, $j, k = 1, 2, 3$ so that the one parameter family $\gamma_{j,k}(s)$ exists for all $0 \leq s < \hat{s}_{j,k}$. If $\hat{s}_{j,k} < 1$, then the homoclinic family loses transversality and disappears at $s = \hat{s}_{j,k}$. If $\hat{s} = 1$, then the homoclinic survives all the way to $\mathfrak{D}$. In any event, the number $\hat{s}_{j,k}$ provides a measure of the robustness of $\gamma_{j,k}$.

The general principle informing our work in this section is that numerical continuation algorithms are based on Newton's method, and Newton's method must break down near a bifurcation by the implicit function theorem. So, if $\hat{s}_{j,k} < 1$, then the numerical continuation

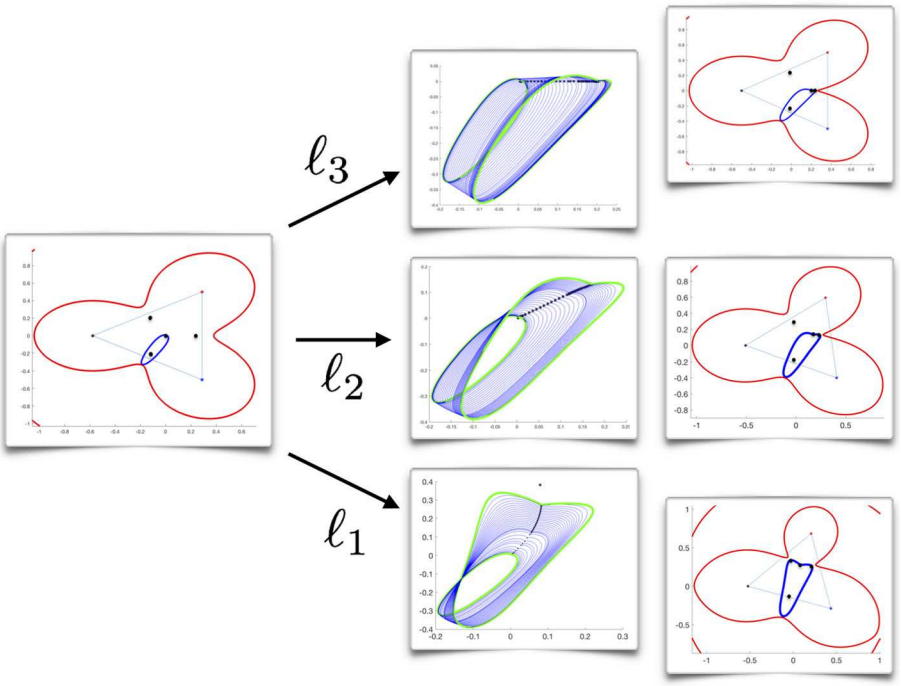

Fig. 6 Numerical continuation of γ_1**:** continuations along $\ell_{1,2,3}(s)$ are successful roughly 74%, 92%, and 97% of the way to the critical curve $\mathfrak{D}$, respectively. The left frame illustrates the homoclinic orbit γ_1 (blue curve) in the triple Copenhagen problem, that is, when the parameters are $v_0 = (1/3, 1/3, 1/3)$. The red curve is the zero velocity curve for the L_0 energy level. The three middle frames illustrate the results of numerical continuation of γ_1 along the parameter lines $\ell_{1,2,3}(s)$. In each case the initial and final numerically computer homoclinics are colored green and the intermediate homoclinics are colored blue. The step size in the continuation algorithm is chosen adaptively, so that the blue homoclinic orbits are not uniformly spaced. The black dots illustrate the numerical continuation of the libration points L_0. The three right frames illustrate the terminal homoclinic orbits $\gamma_{1,k}(s)$ for $s \approx \hat{s}_{1,k}$, $k = 1, 2, 3$ with the corresponding zero velocity curves. In each of the three frames on the right we see that there are four inner libration points. That is, the numerical continuation did not reach the critical curve $\mathfrak{D}$

of $\gamma_{j,k}$ must break down before we reach this critical value. On the other hand, homoclinic orbits can undergo other types of bifurcations, such as homoclinic doubling (Kokubu 1988) or the Belyakov–Devaney bifurcation discussed in Sect. 1.4. Then, the breakdown of numerical continuation provides an indicator that the homoclinic is undergoing some kind of bifurcation, and hence provides a lower bound on the value of $\hat{s}_{j,k}$ and the disappearance of the homoclinic. We also remark that numerical continuation breaks down near $\mathfrak{D}$ because the underlying equilibrium undergoes a bifurcation.

2.1 Continuation of the γ_1 family

Applying the strategy of the previous section starting from γ_1 leads to the following results. We find that the continuation algorithm breaks down near $s = 0.74$ when we continue along the $\ell_1(s)$ parameter line, near $s = 0.9247$ along the $\ell_2(s)$ parameter line, and near $s = 0.974$ along the $\ell_3(s)$ parameter line. The results are illustrated graphically in Fig. 6, and suggest

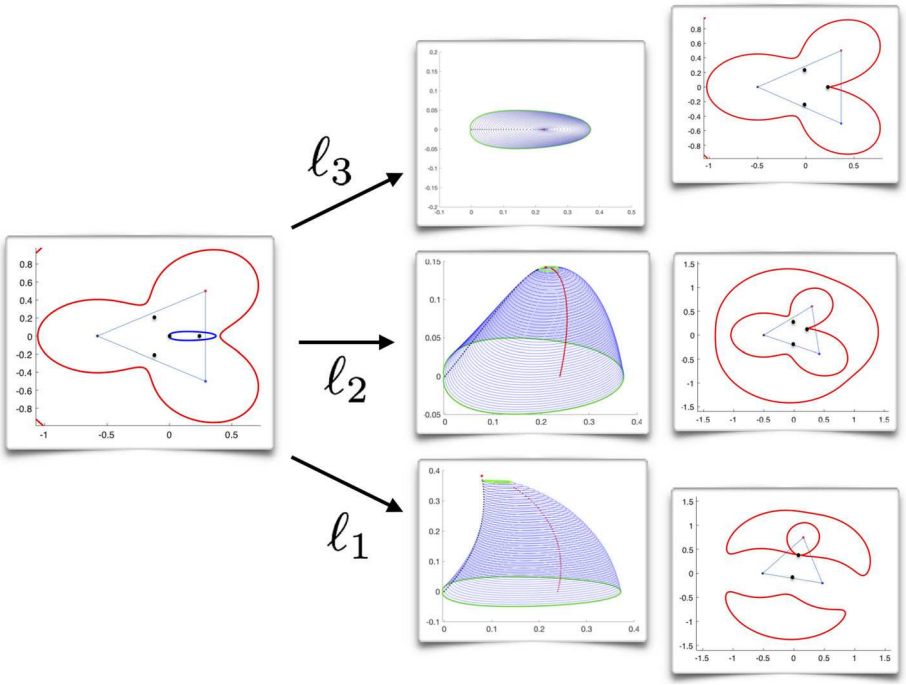

Fig. 7 Continuation of the γ_2 family: continuations along $\ell_{1,2,3}(s)$ are successful almost 100% of the way to the critical curve $\mathfrak{D}$. Objects are colored as described in the caption of Fig. 6. In each of the middle frames one sees the homoclinic orbits shrinking to zero as L_0 approaches L_2. Continuation of the L_2 family is shown in the bottom and middle frames (red curves). Since the families continue almost all the way to $s = 1$ the right frames show the zero velocity curves at $v_{c_{1,2,3}}$ when the homoclinics have vanished

that the $\gamma_{1,1}(s)$ family is the least robust, $\gamma_{1,3}(s)$ the most robust, and $\gamma_{1,2}(s)$ is in between. The results suggest also that none of the γ_1 continuations survive all the way to the critical curve $\mathfrak{D}$. Rather, in the terminology of Sect. 1.4, γ_1 appears to undergo a type IV bifurcation along each of the parameter lines. More precisely, we conjecture that the numerical lower bounds

$$0.74 < \hat{s}_{1,1}, \qquad 0.9247 < \hat{s}_{1,2} \qquad \text{and} \qquad 0.974 < \hat{s}_{1,3},$$

hold along the $\ell_{1,23}(s)$ parameter lines.

2.2 Continuation of the γ_2 family

Continuation of the γ_2 family appear to be more straight forward, as in every case the continuation succeeds until $s \approx 1$, breaking down only when L_2 approaches L_0 and the homoclinics become very small (distance on the order of 10^{-4}) when they become difficult to distinguish numerically. The results are illustrated in Fig. 7, and appear to indicate that the γ_2 families are as robust as possible. Based on these observations we conjecture that

$$\hat{s}_{2,1} = \hat{s}_{2,2} = \hat{s}_{2,3} = 1.$$

That is, along the parameter lines $\ell_{1,2,3}(s)$, the γ_2 families continue all the way to the critical set $\mathfrak{D}$. Indeed, we will see in Sect. 4 that this conjecture is further supported by normal form calculations at L_c.

2.3 Continuation of the γ_3 family

In considering the γ_3 family it is first useful to exploit the symmetries of the problems, in order that some of the results already discussed can be recycled. For example, when $m_2 = m_3$, the system is symmetric about the x axis and that $\gamma_{3,3}(s)$ family is obtained from the $\gamma_{1,3}(s)$ family by reflection. Then, based on the results presented in Sect. 2.1, the γ_3 family inherit the conjecture

$$0.974 < \hat{s}_{3,3} = \hat{s}_{1,3},$$

suggesting again a type IV bifurcation in the terminology of Sect. 1.4.

Similarly, when $m_1 = m_2$, the system has symmetry about the line through the third primary bisecting the opposite edge of the Lagrangian triangle in phase space. Thanks to this symmetry, the $\gamma_{3,1}(s)$ homoclinic family is obtained by reflection of $\gamma_{2,1}(s)$ family, and by the results in Sect. 2.2 we inherit the conjecture that

$$\hat{s}_{3,1} = \hat{s}_{2,1} = 1.$$

Recall also that the critical bifurcation at v_{c_1} is a pitch fork, wherein the libration points L_0, L_2 and L_3 collide. Then, the $\gamma_{3,1}(s)$ family shrinks to zero as L_3 approaches L_0, exactly as the $\gamma_{2,1}(s)$ family shrinks as L_2 approaches L_0. It follows that $\hat{s}_{3,1} = \hat{s}_{2,1} = 1$, and the $\gamma_{3,1}(s)$ family is as robust as possible. Indeed, this is the picture predicted by the normal form for the pitch fork bifurcation as discussed in Sect. 1.4.

Finally, we report that numerical continuation of the $\gamma_{3,2}$ family succeeds almost 97% of the way to v_{c_2} along the $\ell_2(s)$ parameter line. Based on this we have the bound

$$0.97 < \hat{s}_{3,2}.$$

More insight into the fate of the $\gamma_{3,2}$ family is obtained by considering the normal form calculations in Sect. 4. The results of all three numerical continuations are summarized in Fig. 8.

Remark 1 *(Belyakov–Devaney bifurcations)* It is worth remarking that each of the continuation families $\gamma_{j,k}(s)$ undergoes a type II bifurcation before the numerical continuation breaks down. That is, in each case the underlying equilibrium solution $L_0(s)$ changes stability form a bi-focus to a saddle with real distinct eigenvalues for $s < \hat{s}_{j,k}$. This suggests that the Belyakov–Devaney bifurcation is universal for the $\gamma_{1,2,3}$ families. We note that while this bifurcation effects the computation of the stable/unstable manifolds of L_0, the homoclinics do not break down there, and we can arrange that the numerical continuation "jumps over" the bifurcation.

Remark 2 *(A point of clarification regarding the "false" heteroclinic cycles)* Upon close inspection of the right three frames of Fig. 6 we note that in each of the three cases considered L_2 appears to lie on the critical γ_1 curve. This could suggest that γ_1 terminates in a heteroclinic bifurcation, resulting in a connection from L_0 to L_2 and back. However, the proposed heteroclinic cycle is impossible, as L_0 and L_2 are in different energy levels when γ_1 is critical. In fact L_0 and L_2 are only ever in the same energy level when they collide and disappear on the critical curve $\mathfrak{D}$. By computing the tangent vectors along γ_1 we find that it

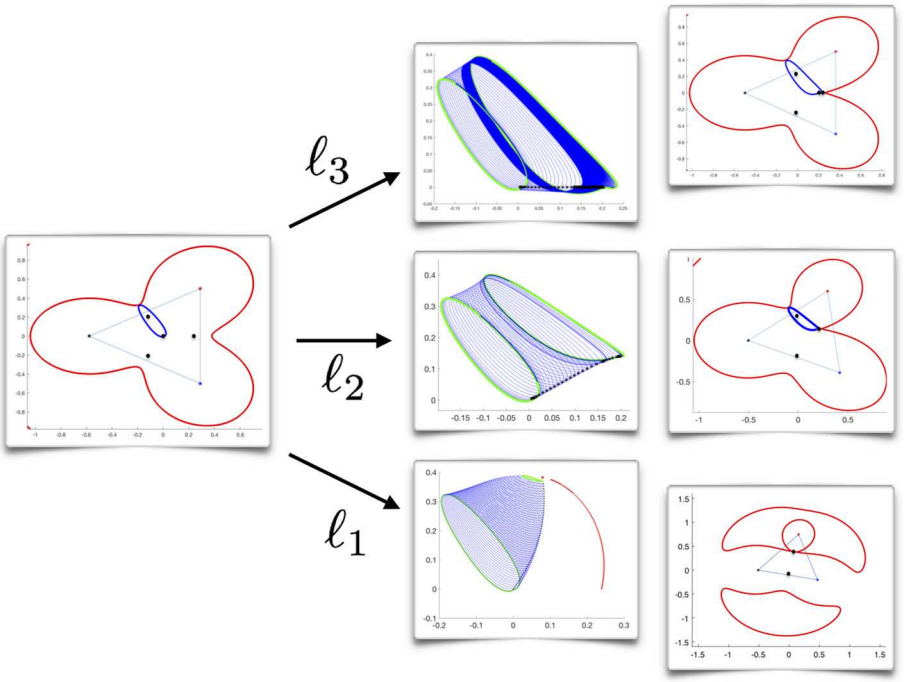

Fig. 8 Numerical continuation of the γ_3 basic homoclinic: continuations along $\ell_{1,2,3}(s)$ are successful roughly 100%, 97%, and 97% of the way to the critical curve $\mathfrak{D}$, respectively . Objects are colored as described in the caption of Fig. 6. The left frame illustrates the homoclinic orbit γ_3 (blue curve) when the parameters are $v_0 = (1/3, 1/3, 1/3)$. The black dots in the middle three frames illustrate the numerical continuation of the libration points L_0, while the red dots in the bottom middle frame illustrate the continuation of L_2. The top and middle right frames illustrate the terminal homoclinic orbits $\gamma_{3,k}(s)$ for $s \approx \hat{s}_{3,k}$, $k = 1, 2$ with the corresponding zero velocity curves. Note that in both cases the libration points L_0 and L_2 have not quite collided, but that the homoclinics are difficult to continue any further. (In the middle right frame it is difficult to distinguish L_0 and L_2 graphically at this resolution.) The bottom right frame, on the other hand, illustrates the zero velocity curves in the critical energy level for system parameters v_{c_3}, where L_0, L_2, L_3 have collided, and the homoclinic family appears to have shrunk to zero

"passes over" L_2 with nonzero velocity so that the suggestion of a heteroclinic orbit seen in Fig. 6 is an effect of projecting into the plane.

3 The blue sky test: continuation of the planar Lyapunov families of $L_{1,2,3}$

In this section we discuss calculations which can be used to refine the results of Sect. 2. The idea is based on the fact, already mentioned in the introduction, that γ_j, $j = 1, 2, 3$ appear as limits of the planar Lyapunov families associated with saddle $\times$ center libration points L_j, $j = 1, 2, 3$. Our experience suggests that this relationship is very stable with respect to parameter perturbations. Indeed, let $L_{j,k}(s)$ denote the continuation of L_j along the parameter line $\ell_k(s)$. For $0 \leq s \leq \hat{s}_{j,k}$ we always find that $\gamma_{j,k}(s)$ is always the limit of the planar Lyapunov family associated with $L_{j,k}(s)$, $j, k = 1, 2, 3$. To put it another way,

the tube of periodic orbits attached to $\gamma_{j,k}(s)$ appears to change its limit behavior only with the loss of transversality and disappearance of the homoclinic itself.

In this section we proceeded as if the converse of this statement holds. That is, when the planar Lyapunov family associated with $L_{j,k}(s)$ does not accumulate to a homoclinic at $L_{0,k}(s)$, we take this as an indication that the $\gamma_{j,k}(s)$ homoclinic family has terminated. Hence, when we numerically locate such an $s \in (0, 1)$, we assume that $s > \hat{s}_{j,k}$. Since the continuation-based methods of Sect. 2 provide lower bounds on $\hat{s}_{j,k}$, the methods based on blue sky catastrophes developed in this section provide upper bounds and hence numerical enclosures of the bifurcation parameter.

Of course this procedure is indicative rather than definitive, as the assumptions are based on heuristics rather than mathematically rigorous results. A change in the terminal behavior of a tube indicates only that some bifurcation has occurred in the homoclinic family, not necessarily that it has disappeared. Nevertheless, when used in conjunction with the continuation methods of Sect. 2 and the normal form/center manifold analysis of Sect. 4, we obtain a compelling narrative describing the global dynamics. We return to this point in Sect. 5.

3.1 Blue skies for the γ_1 family

Recall from Sect. 2 that the $\gamma_{1,1}(s)$ family enjoys the lower bound $0.74 < \hat{s}_{1,1}$. In other words, we are fairly confident that family exists along more than 74 percent of the $\ell_1(s)$ parameter line. We apply numerical continuation (with respect to the energy) to the planar Lyapunov family associated with $L_{1,1}(0.74)$, and recover the homoclinic connection to $L_{0,1}(0.74)$ already computed by mass parameter continuation in the previous section.

Now, taking $s = 0.78$ we numerically continue the planar Lyapunov family associated with $L_{1,1}(0.78)$ and find that the periodic orbits do not accumulate to an orbit homoclinic to $L_{0,1}(0.78)$. Instead, we find that we can continue the periodic orbits up to and beyond the energy level of $L_{0,1}(0.78)$. The Lyapunov family appears to eventually accumulate on an orbit which collides with the third primary. This another piece of evidence supporting the claim that the $\gamma_{1,1}(s)$ family terminates nearby. Indeed, we appear to have the bound $\hat{s}_{1,1} < 0.78$. Combining this with the results discussed in Sect. 2.1, we conjecture that

$$\hat{s}_{1,1} \in (0.74, 0.78).$$

The results of the calculation just discussed are illustrated in Fig. 9. When we perform similar calculations for the $\gamma_{1,2}(s)$ and $\gamma_{1,3}(s)$ families of homoclinic orbits, and combine these with the lower bounds already obtained Sect. 2, we obtain the enclosures

$$\hat{s}_{1,2} \in (0.9, 0.95)$$
$$\hat{s}_{1,3} \in (0.97, 1).$$

The results are illustrated in Figs. 10 and 11.

3.2 Blue skies for the γ_2 family

Since the γ_2 family appears to disappear with L_2 in the saddle node bifurcation, the kind of blue sky analysis discussed above is not available here. Indeed, for s near one the L_2 Lyapunov families do converge to the small homoclinics seen in Sect. 2, and at the critical energy L_2 is gone so that there are no planar Lyapunov families to study. The γ_2 family is much more amenable to the local analysis performed in Sect. 4.

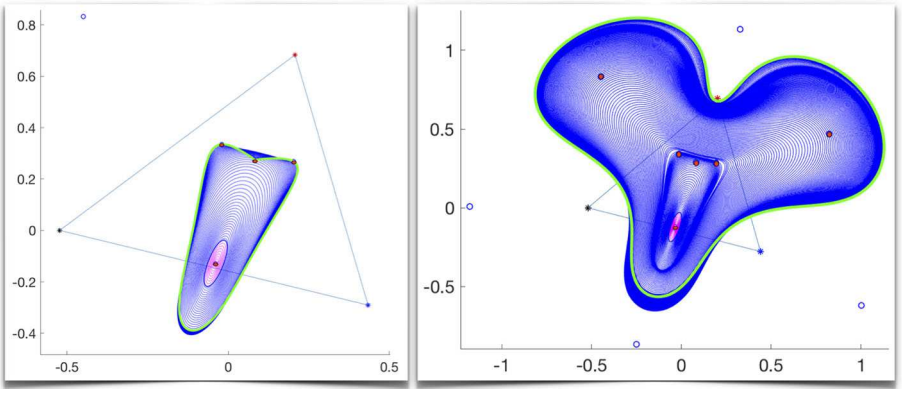

Fig. 9 Blue sky catastrophes along the $\ell_1(s)$ parameter curve: The left frame illustrates the CRFBP with parameter values $\ell_1(0.74)$. We study the blue sky catastrophe for the planar Lyapunov family of $L_{1,1}(0.74)$, and see that the periodic orbits accumulate to an orbit homoclinic to $L_{0,1}(0.74)$—in fact the same homoclinic orbit depicted in the bottom right frame of Fig. 6, computed by numerical continuation along the $\ell_1(s)$ parameter curve starting from γ_1. The homoclinic orbit is represented by the green curve, periodic orbits on the center manifold of $L_{1,1}(0.74)$ are represented by the magenta curves, and periodic orbits obtained by numerical continuation from the center manifold are represented by blue curves. The calculation suggests that $\hat{s}_{1,1} > 0.74$. The right frame illustrates the planar Lyapunov family of $L_{1,1}(0.78)$, again computed by numerical continuation from the center manifold. The planar Lyapunov family appears to terminate at a collision with the small primary body. The fact that the Lyapunov family does not accumulate to an orbit homoclinic to $L_{0,1}(0.78)$ suggests that $\hat{s}_{1,1} < 0.78$

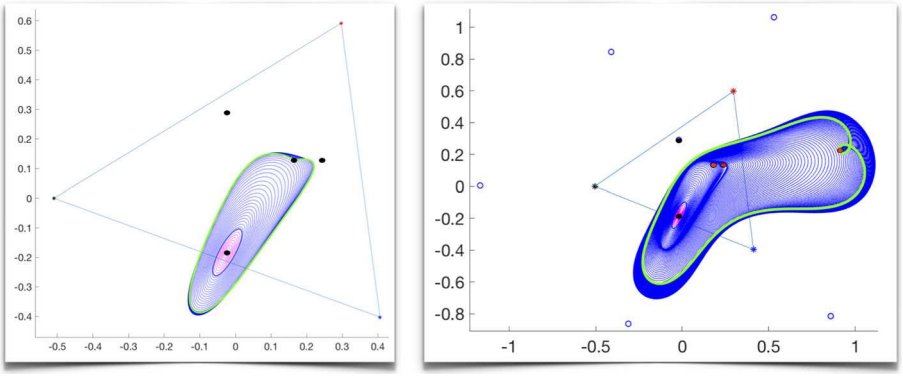

Fig. 10 Blue sky catastrophes on the $\ell_2(s)$ parameter curve: The left frame illustrates the CRFBP with parameter values $\ell_2(0.9)$. We study the blue sky catastrophe for the planar Lyapunov family of $L_{1,2}(0.9)$ and reasoning just as in the caption of Fig. 9 conclude that $\hat{s}_{1,2} > 0.9$. Similarly, the right frame illustrates the planar Lyapunov family of $L_{1,2}(0.95)$, and suggests that $\hat{s}_{1,2} < 0.95$

3.3 Blue skies for the γ_3 family

As already noted in Sect. 2, the γ_3 family exhibits somewhat more complicated behavior than the γ_1 family—which never persists to $\mathfrak{D}$, and the γ_2 family—which always does. The behavior of the γ_3 family on the $\ell_1(s)$ and $\ell_3(s)$ parameter lines is forced by symmetry. So $\gamma_{3,3}(s)$ has the same terminal behavior as $\gamma_{1,3}(s)$, as one is obtained from the other by

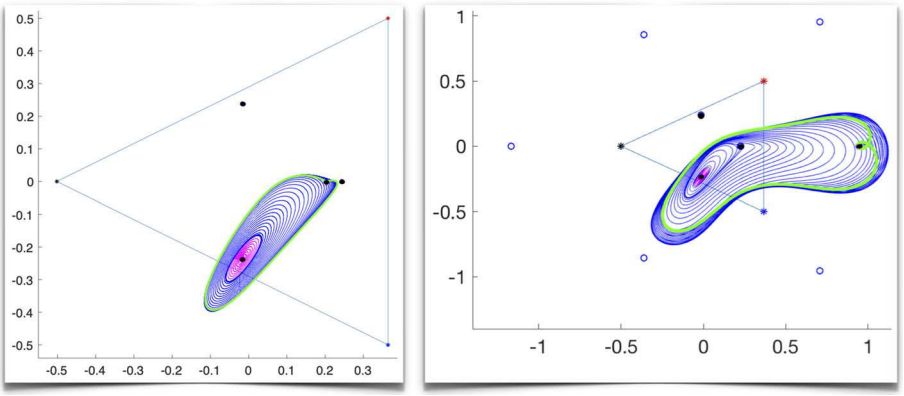

Fig. 11 Blue sky catastrophes on the $\ell_3(s)$ parameter curve: The left frame illustrates the CRFBP with parameter values $\ell_3(0.97)$. We study the blue sky catastrophe for the planar Lyapunov family of $L_{1,3}(0.97)$ and reasoning just as in the caption of Fig. 9 conclude that $\hat{s}_{1,3} > 0.97$. Similarly, the right frame illustrates the planar Lyapunov family of $L_{1,3}(1)$, and suggests that $\hat{s}_{1,3} < 1$

reflection about the x axis. From this we have that

$$\hat{s}_{3,3} = \hat{s}_{1,3} \in (0.97, 1),$$

thanks to the results for γ_1 already reported. Similarly, the $\gamma_{3,1}$ family is related to the $\gamma_{2,1}$ family by a reflection. Then, the study of the $\gamma_{3,1}$ family is amenable to normal form analysis, as already remarked for the γ_2 family.

Finally, recall from Sect. 2 that the $\gamma_{3,2}(s)$ family continued 97 percent of the way to $\mathfrak{D}$. We remark that the blue sky test for $\gamma_{3,2}(s)$ is inconclusive, in the sense that for s values near one on the $\ell_2(s)$ parameter curve the numerical continuation of the periodic family breaks down near the L_c energy level. It is unclear what this breakdown indicates—Does the periodic family accumulate to a homoclinic at L_c? Or would a more computational effort show that the periodic family continues past the L_c energy level? Again, since the problem occurs near $\mathfrak{D}$, the normal form analysis in Sect. 4 is seen to resolve the issue.

4 Results of center manifold/normal form calculations

Instead of numerically following homoclinic orbits or Lyapunov families from the triple Copenhagen problem to the bifurcation curve, we can start our calculations at the bifurcation point itself. That is, we compute the normal form r of the center dynamics along the parameter lines $\ell_{1,2,3}(s)$. As we start at the bifurcation point instead of at the triple Copenhagen problem, we reverse the orientation on the curves, and consider the parameter lines $\hat{\ell}_{1,2,3}(s) = \ell_{1,2,3}(1-s)$ instead. For the saddle node bifurcation, we have the normal form

$$r : \mathbb{R} \times \mathbb{R}^2 \to \mathbb{R}^2, (s, x, y) \mapsto (y, s + \alpha_1 x^2),$$

for the conjugate vector field r on the center manifold. With the normal form, we can confirm that $\hat{s}_{2,k} = 1$ for $k = 2, 3$, see Fig. 12. By calculating higher-order terms of the conjugate vector field, we can determine whether the γ_3 orbit lies on the center manifold. The calculated vector fields are given in Table 1. If we truncate the vector field r to third order, its phase

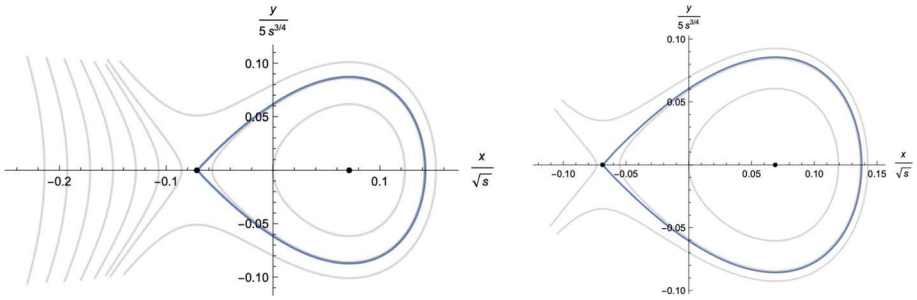

Fig. 12 Small orbits near the saddle node bifurcation: In the left figure, we plotted several orbits for the normal form at $\hat{\ell}_2(10^{-13})$, with the blue line the approximation for $\gamma_{2,2}(1-10^{-13})$. All orbits on the left side of L_0 decrease to $x=-\infty$. In the right figure, we plotted several orbits for the normal form at $\hat{\ell}_3(10^{-13})$, with the blue line the approximation for $\gamma_{2,3}(1-10^{-13})$. Both frames illustrate the conjugate 2 dimensional vector field on the center manifold

Table 1 Normal forms: the calculated constants in the normal forms at v_{c_k} for $k=1,2,3$

	Masses	α_1	α_2	Third-order terms in the y-derivative
Pitchfork	v_{c_1} co-dimension 1	6.93442	−5441.04	–
	v_{c_1} co-dimension 2	6.93442	−5441.04	–
Saddle node	v_{c_2}	−196.451	–	$20818.5x^3$
	v_{c_3}	−211.138	–	$24498.1x^3$

portrait does contain two fixed points, but does not contain a homoclinic orbit for small values of s. This suggest that if $\gamma_{3,2}$ persists until $\mathfrak{D}$, it does not lie on the local center manifold.

For $\hat{\ell}_1(s)$, the normal form of the conjugate vector field is given by

$$r:\mathbb{R}\times\mathbb{R}^2\to\mathbb{R}^2,\ (s,x,y)\mapsto(y,\alpha_1 sx+\alpha_2 x^3),$$

which will confirm that $\hat{s}_{2,1}=1$ and $\hat{s}_{3,1}=1$, see Fig. 13. Instead of computing the normal form of the co-dimension one pitchfork bifurcation at v_{c_1}, we can compute the normal form of the co-dimension two bifurcation at v_{c_1}. Then, the normal form would be, for instance (Buono et al. 2005),

$$r:\mathbb{R}^2\times\mathbb{R}^2\to\mathbb{R}^2,\ (s,t,x,y)\mapsto(y,t+\alpha_1 sx+\alpha_2 x^3).$$

With this normal form, we can recover part of $\mathfrak{D}$ near v_{c_1}, and show the persistence of γ_3 until $\mathfrak{D}$ for v_c near v_{c_1}, see Fig. 14. The calculated normal forms for both the co-dimension 1 and the co-dimension 2 bifurcation at v_{c_1} are found in Table 1.

4.1 Separation of $\mathfrak{D}$ and the γ_3 family

Following our work in Sects. 2 and 3, we want to better understand the robustness of the γ_3 family. This is especially delicate off the $m_1=m_2$ and $m_2=m_3$ edges of the parameter simplex. Symmetry considerations—combined with the local analysis of the previous section—show that at and near the $m_1=m_2$ edge the γ_3 family is completely robust, surviving all the way to the critical curve $\mathfrak{D}$. On the other hand, symmetry considerations combined with the continuation and blue sky tests of Sect. 2 and 3 suggest that along and

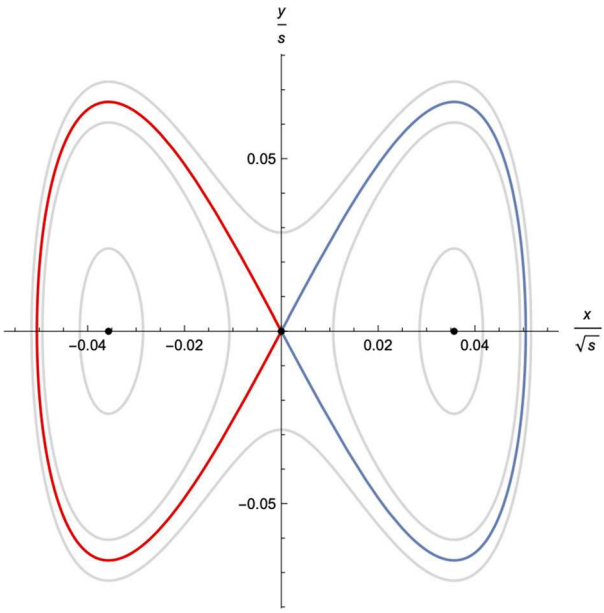

Fig. 13 Small orbits near the Pitchfork bifurcation: Several orbits for the normal form at $\hat{\ell}_1(10^{-13})$. The red and blue line are approximations for $\gamma_{2,1}(1-10^{-13})$ and $\gamma_{3,1}(1-10^{-13})$. The frame illustrates the conjugate two-dimensional vector field on the center manifold

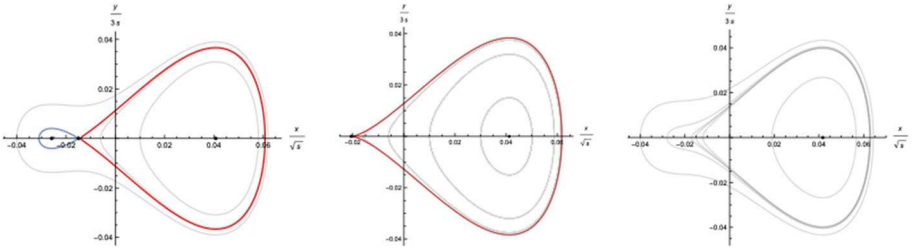

Fig. 14 Persistence of γ_3**:** We show the persistence of γ_3 until the saddle node bifurcation for v_c near v_{pf}. In the left frame, we have $(m_1, m_2, m_3) \in \mathfrak{S}_I$ near v_{pf} but away from the $m_1 = m_2$ edge. We see the small homoclinic orbit γ_2 and the large homoclinic orbit γ_3 illustrated by blue and red curves, respectively. In the middle frame we have $(m_1, m_2, m_3) \in \mathfrak{D}$ near v_{pf}. Here L_0 and L_2 have collided at L_c, yet we still see γ_3, which is illustrated by the red curve. In the right frame, we have $(m_1, m_2, m_3) \in \mathfrak{S}_{II}$ near v_{pf} but away from the $m_1 = m_2$ edge. As L_c has disappeared, γ_3 has become a periodic orbit around L_3. All frames illustrate the conjugate two-dimensional vector field on the center manifold

near the $m_2 = m_3$ edge, the γ_3 family terminates before the $\mathfrak{D}$ curve. Taken together, this suggests that γ_3 must exhibit some transitional behavior, some co-dimension two bifurcation, along $\mathfrak{D}$.

We attempt to resolve this picture as follows:

1. We use Newton's method to find m_2, x_0 and y_0 for fixed m_1 such that $(m_1, m_2, 1-m_1-m_3) \in \mathfrak{D}$, with corresponding libration point is $L_c = (x_0, 0, y_0, 0)$.,
2. We choose $K_c(x, y) = (x, y)$ and find the Taylor polynomials for the center manifold, the center stable/unstable manifolds, and the (un)stable branch on the center manifold, as shown in Lemmas B.1 to B.3 up to order 15 using radial derivatives,
3. We numerically find the region where the conjugacy Eq. (15) for the center stable/unstable manifold has an error of order 10^{-15} and the stable and unstable branches h_s and h_u are numerically correct for the Taylor polynomials of step 2,

4. We take t_s and t_u such that $h_s(t_s)$ and $h_u(t_u)$ are in the region of step 3. We then find homoclinic orbits by numerically integrating part of the unstable fiber of $h_u(t_u)$ until the stable fiber of $h_s(t_s)$ is reached. We check numerically that the manifolds have a transverse intersection, indicating that we are at a type III global bifurcation.

Here the function k_c is a choice we have to make to find the center manifold at $v_c \in \mathfrak{D}$. We refer the reader to Appendix B for background on the center manifold, and Lemma B.1 in particular to see why we have to choose k_c. Furthermore, the branches h_s and h_u parameterize the (un)stable orbit on the center manifold, see Fig. 17.

For $m_1 \in \{0.426, 0.427, 0.428, 0.429, 0.430\}$, we compute the homoclinic for L_c around L_3. See Fig. 15. For all five values of m_1, we find that the homoclinic orbit exists, and it leaves the unstable manifold close to the center unstable branch. On the other hand, the homoclinic orbits enter the stable manifold further away from the stable branch on the center manifold when we decrease m_1. To be more precise, for all values of m_1 we look where on the stable fiber of $h_s(t_s)$ the homoclinic orbit enters the stable manifold. As m_1 decreases, we see that the orbit enters the stable manifold further away from $h_s(t_s)$ on its stable fiber. Equivalent, the homoclinic orbit enters the stable fiber of $h_s(t)$ at fixed distance from $h_s(t)$ for decreasing values of t as m_1 decreases. We conjecture that the γ_3 family split from the critical curve $\mathfrak{D}$ when the homoclinic orbit around L_3 enters the stable manifold along the stable direction.

In the right frame of Fig. 16, we integrated points on the boundary of the stable manifold for $m_1 = 0.426$, and we see three different kinds of behavior. The single blue orbit in the lower half of the figure is the backward integration of the stable branch on the center manifold, and all other orbits lie on a stable fiber. Near the equilibrium, the orbits on the stable fibers decay exponentially fast toward the stable branch on the center manifold. In other words, in backward time the orbits on the stable fibers diverge exponentially fast away from the stable branch. This explains why the stable branch on the center manifold lies isolated from the orbits on the stable fibers. The orbits ending on the stable fibers exhibit two different kinds of behavior. The black orbits all come toward L_3 from the right, make a bend before L_3, and end up in the stable manifold of L_c. The blue orbits all come from the left of L_3, passing above L_3 before making a bend toward the stable manifold. Due to this dichotomy, in particular the blue orbits passing above L_3, we might find a homoclinic orbit around L_3 when $m_1 = 0.426$. In fact, we find such a homoclinic orbit which is shown in Fig. 15. In particular, in Fig. 15 we only plot a small region of the stable manifold in which the homoclinic orbit lies.

On the contrary, in the left figure of Fig. 16, we integrated several points on the boundary of the stable manifold for the parameter set v_{c_2}. Here the black line is the backward integration of the stable branch of the center manifold. All other orbits end up on a stable fiber and exhibit the same qualitative behavior. They come toward L_3 from the left, but pass underneath L_3 and finally end up in the stable manifold.

Since we do not see the dichotomy nor orbits passing above L_3 for the parameters v_{c_2} that we did see for $m_1 = 0.426$, we qualitatively rule out that there is a short homoclinic orbit around L_3 for the parameter values v_{c_2}. Any homoclinic around L_3 will occur on longer time scales than the short homoclinics in the γ_3 family. This shows that $\hat{s}_{3,2} < 1$.

4.2 Additional homoclinic at $\mathfrak{D}$

We now expand on the ideas of the previous section, to study longer homoclinic orbits at L_c. Again we consider symmetric and non-symmetric cases. In the symmetric case step 1 will be modified, as for v_{c_3} we want to impose that $m_2 = m_3$, instead of fixing m_1 a priori. For v_{c_1}, we have shown at the beginning of Sect. 4 that the bifurcation is a supercritical pitchfork

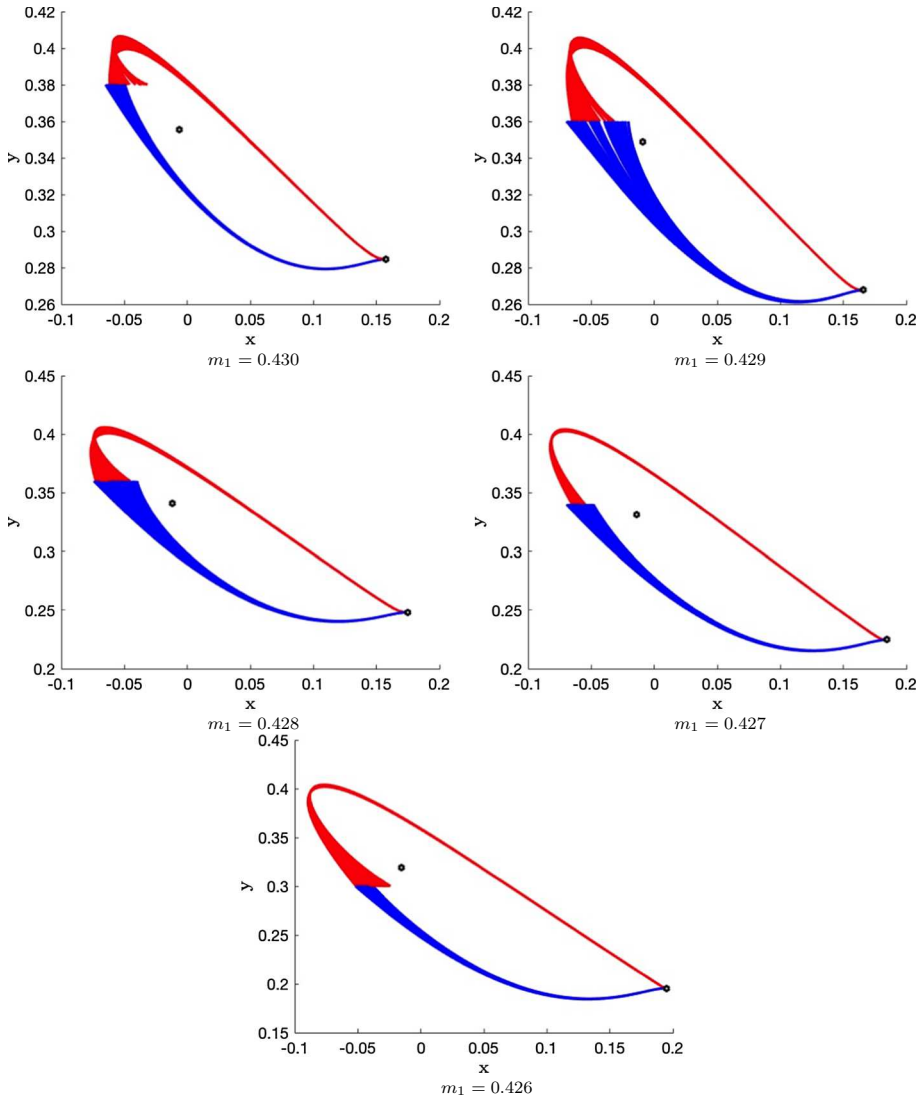

Fig. 15 Short homoclinics around L_3 on $\mathfrak{D}$**:** For different values of m_1 we find a short homoclinic orbit for L_c at parameter values $(m_1, m_2, 1 - m_1 - m_2) \in \mathfrak{D}$. The red surface is the backward flow of part of the edge of stable manifold, and the blue surface is the forward flow of part of the edge of the unstable manifold. In all 5 cases, there is a transverse intersection between the stable and unstable manifold on the $y =$ constant level set with $\dot{y}$ positive, and each of the orbits has a shape suggesting they are continuations of γ_3 in the triple Copenhagen problem

bifurcation: Thus, there will be no (un)stable solution branch on the center manifold. In fact, we show that the constant $\mathscr{E}$ from Lemma B.2 is zero at v_{c_1}. As a consequence, the stable and unstable manifold of L_{pf} are both of dimension 1, and we expect no transverse intersection between them. Therefore, we only look for homoclinics for L_c at parameter values v_{c_2} and v_{c_3}.

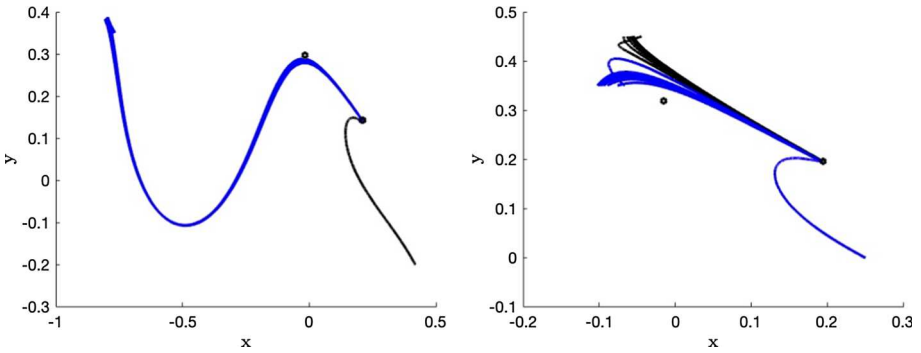

Fig. 16 Qualitative behavior of the stable manifold: left frame plots the backward integration of the edge of the stable manifold for parameter values $v_{c_2} \in \mathfrak{D}$. Right frame plots the backward integration of the edge of the stable manifold for the parameter values $(m_1, m_2, 1 - m_1 - m_2) \in \mathfrak{D}$ for $m_1 = 0.426$

4.3 The pitchfork bifurcation at v_{c_1}

To show that the constant $\mathscr{E}$ from Lemma B.2 is 0, we find the symmetry of f. For notational convenience, we apply the translation $T(x, y) = (x - (x_1 + x_2)/2, y - (y_1 + y_2)/2)$ to our dynamical system and hence, the positions of the planets become

$$\hat{x}_1 = \frac{-1}{4M}, \qquad \hat{y}_1 = \frac{\sqrt{3}(1-2m_1)}{4M},$$
$$\hat{x}_2 = \frac{1}{4M}, \qquad \hat{y}_2 = \frac{-\sqrt{3}(1-2m_1)}{4M},$$
$$\hat{x}_3 = \frac{3-6m_1}{4M}, \qquad \hat{y}_3 = \frac{\sqrt{3}}{4M}.$$

Here $M = \sqrt{m_2^2 + m_2 m_3 + m_3^3} = \sqrt{1 - 3m_1 + 3m_1^2}$ when $m_1 = m_2$. Now we see that when $m_1 = m_2$ we have that $(\hat{x}_1, \hat{y}_1)$, and therefore, also $(\hat{x}_2, \hat{y}_2)$, is perpendicular to $(\hat{x}_3, \hat{y}_3)$. Let Θ be the rotation matrix such that the positive $\hat{y}$-axis is rotated onto the normalized vector $(\hat{x}_3, \hat{y}_3)$. Then, Θ is given by the formula

$$\Theta(x, y) = 2x\hat{\mathbf{x}}_2 + \frac{2y}{\sqrt{3}}\hat{\mathbf{x}}_3.$$

Note that $\hat{\mathbf{x}}_1 = -\hat{\mathbf{x}}_2$ and that $\hat{\mathbf{x}}_2$ and $\hat{\mathbf{x}}_3$ are perpendicular. Then, the term $-(1-2m_1)\hat{\mathbf{x}}_3$ in the first norm is due to the fact that the translation T can be written as $T(\mathbf{x}) = \mathbf{x} + (1 - 2m_1)\hat{\mathbf{x}}_3$,

$$\begin{aligned}\Omega(T^{-1}(\Theta(-s,t))) &= \frac{1}{2}\| - 2s\hat{\mathbf{x}}_2 + \frac{2t}{\sqrt{3}}\hat{\mathbf{x}}_3 - (1-2m_1)\hat{\mathbf{x}}_3\|_2^2 \\ &\quad + \sum_{i=1}^{3} \frac{m_i}{\| - 2s\hat{\mathbf{x}}_2 + \frac{2t}{\sqrt{3}}\hat{\mathbf{x}}_3 - \hat{\mathbf{x}}_i\|_2} \\ &= \frac{1}{2}\|2s\hat{\mathbf{x}}_2 + \frac{2t}{\sqrt{3}}\hat{\mathbf{x}}_3 - (1-2m_1)\hat{\mathbf{x}}_3\|_2^2 + \frac{m_3}{\| - 2s\hat{\mathbf{x}}_2 + \frac{2t}{\sqrt{3}}\hat{\mathbf{x}}_3 - \hat{\mathbf{x}}_3\|_2} \\ &\quad + \frac{m_1}{\| - 2s\hat{\mathbf{x}}_2 + \frac{2t}{\sqrt{3}}\hat{\mathbf{x}}_3 - \hat{\mathbf{x}}_1\|_2} + \frac{m_2}{\| - 2s\hat{\mathbf{x}}_2 + \frac{2t}{\sqrt{3}}\hat{\mathbf{x}}_3 - \hat{\mathbf{x}}_2\|_2}\end{aligned}$$

$$
\begin{aligned}
&= \frac{1}{2}\|2s\hat{\mathbf{x}}_2 + \frac{2t}{\sqrt{3}}\hat{\mathbf{x}}_3 - (1-2m_1)\hat{\mathbf{x}}_3\|_2^2 + \frac{m_3}{\|2s\hat{\mathbf{x}}_2 + \frac{2t}{\sqrt{3}}\hat{\mathbf{x}}_3 - \hat{\mathbf{x}}_3\|_2} \\
&\quad + \frac{m_2}{\|2s\hat{\mathbf{x}}_2 + \frac{2t}{\sqrt{3}}\hat{\mathbf{x}}_3 - \hat{\mathbf{x}}_2\|_2} + \frac{m_1}{\|2s\hat{\mathbf{x}}_2 + \frac{2t}{\sqrt{3}}\hat{\mathbf{x}}_3 - \hat{\mathbf{x}}_1\|_2} \\
&= \Omega(T^{-1}(\Theta(s,t))).
\end{aligned}
$$

We define $\Phi(s,t) \overset{\text{def}}{=} \Omega(T^{-1}(\Theta(s,t)))$, and our bifurcation point lies in translated coordinates on the line $\hat{\mathbf{x}}_3$, i.e., $\Omega(x_0, y_0) = \Phi(0,t)$ for some $t \in \mathbb{R}$. From the symmetry $\Phi(-s,t) = \Phi(s,t)$ we obtain

$$
\begin{aligned}
\Phi_s(0,t) &= -\Phi_s(0,t) = 0, \\
\Phi_{st}(0,t) &= -\Phi_{st}(0,t) = 0, \\
\Phi_{sss}(0,t) &= -\Phi_{sss}(0,t) = 0.
\end{aligned}
$$

Let $\lambda = \sqrt{3}(1-2m_1) = \sqrt{3}m_3$. Using the chain rule we have

$$
2M\Phi_s(0,t) = \Omega_x - \lambda\Omega_y = 0, \tag{6}
$$

$$
4M^2\Phi_{st}(0,t) = \lambda\Omega_{xx} + (1-\lambda^2)\Omega_{xy} - \lambda\Omega_{yy} = 0, \tag{7}
$$

$$
8M^3\Phi_{sss}(0,t) = \Omega_{xxx} - 3\lambda\Omega_{xxy} + 3\lambda^2\Omega_{xyy} - \lambda^3\Omega_{yyy} = 0. \tag{8}
$$

Furthermore, since we are at a bifurcation point, we also have $\Omega_{xx}\Omega_{yy} = \Omega_{xy}^2$; hence, Eq. (7) becomes

$$
\lambda\Omega_{xx}^2 + (1-\lambda^2)\Omega_{xy}\Omega_{xx} - \lambda\Omega_{xy}^2 = 0.
$$

Therefore, we either have $\Omega_{xx} = \lambda\Omega_{xy}$, thus also $\Omega_{xy} = \lambda\Omega_{yy}$, or $\Omega_{xx} = -\lambda^{-1}\Omega_{xy}$, and also $\Omega_{xy} = -\lambda^{-1}\Omega_{yy}$. To establish that we have $\Omega_{xx} = \lambda\Omega_{xy}$ instead of $\Omega_{xx} = -\lambda^{-1}\Omega_{xy}$, we use Newton's method to find the root of

$$
(\Omega_x(\Theta(0,t)),\ \Omega_{xx}(\Theta(0,t)) - \lambda\Omega_{xy}(\Theta(0,t))),
$$

which defines the bifurcation parameters v_{c_1}—and libration point $L_{c_1} = (\Theta(0,t)_1, 0, \Theta(0,t)_2, 0)$. To see this, from Eq. (6) it follows that $\Omega_y = 0$, i.e., $\Theta((0,t))$ is indeed a fixed point. Furthermore, from Eq. (7) it also follows that $\Omega_{xy} = \lambda\Omega_{yy}$, and hence $\Omega_{xx}\Omega_{yy} = \Omega_{xy}^2$; thus, $\Theta((0,t))$ is not only a fixed point, but the linearization of the vector field at $\Theta((0,t))$ has a double eigenvalue 0.

Exploiting again that $\Omega_{xx} = \lambda\Omega_{xy} = \lambda^2\Omega_{yy}$, the constant $\mathscr{E}$ becomes

$$
\begin{aligned}
\mathscr{E} &= \Omega_{xxx}\Omega_{yy}^3 - 3\Omega_{xxy}\Omega_{yy}^2\Omega_{xy} + 3\Omega_{xyy}\Omega_{yy}\Omega_{xy}^2 - \Omega_{yyy}\Omega_{xy}^3 \\
&= \left(\Omega_{xxx} - 3\lambda\Omega_{xxy} + 3\lambda^2\Omega_{xyy} - \lambda^3\Omega_{yyy}\right)\Omega_{yy}^3 \\
&= \frac{\Omega_{yy}^3}{8M^3}\Phi_{sss}(0,t) \\
&= 0.
\end{aligned}
$$

Hence, Lemma B.2 cannot be applied to find (un)stable solution branches on the center manifold, which further supports the claim that L_c undergoes a pitchfork bifurcation at v_{c_1}.

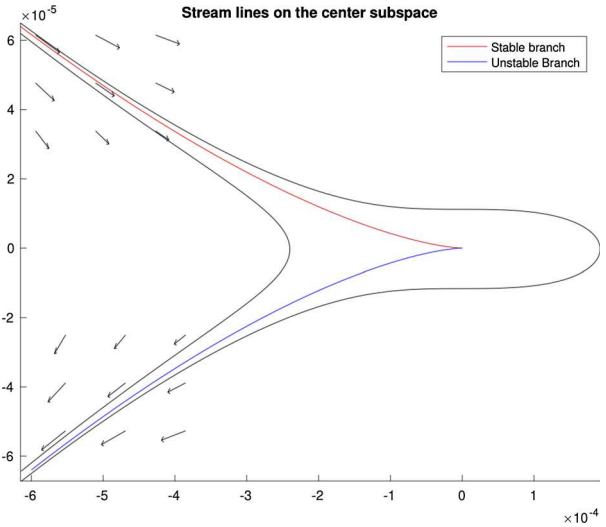

Fig. 17 The approximation of the solution branches on the center manifold for the parameters v_{c_2} on the bifurcation curve

4.4 Generic saddle node bifurcation at v_{c_2}

In our numerical scheme, we use Newton's method to find a root of

$$(\Omega_x, \Omega_y, \Omega_{xx}\Omega_{yy} - \Omega_{xy}^2),$$

where we fix $m_1 = 0.4247$, and consider m_2 as the only parameter. This results in the bifurcation parameters v_{c_2}. In Fig. 17 we plot the Taylor polynomials of the stable and unstable branch, together with two orbits starting close to the stable branch. This allows us to check the branches and take t_s and t_u in step 4 as large as possible. The results of the numerical integration done in step 4 are illustrated in Fig. 18 .

4.5 The non-generic saddle node bifurcation at v_{c_3}

To obtain the bifurcation parameters v_{c_3}, we will exploit that the planar circular restricted four-body problem has symmetry on the edge $m_2 = m_3$. We have $\Omega(x, y) = \Omega(x, -y)$, and thus also $\Omega_x(x, -y) = \Omega_x(x, y)$, $\Omega_y(x, -y) = -\Omega_y(x, y)$, and $\Omega_{xy}(x, -y) = -\Omega_{xy}(x, y)$. In particular, we have $\Omega_y(x, 0) = 0$ and $\Omega_{xy}(x, 0) = 0$. We can therefore in step 1 use Newton' method to find the root of

$$(\Omega_x(x, 0), \Omega_{xx}(x, 0))$$

along $\ell_3(s)$ to obtain the bifurcation parameters v_{c_3} and bifurcation point $L_c = (x_0, 0, 0, 0)$.

The symmetry also motivates us to define the linear map $A : (x, \dot{x}, y, \dot{y}) \mapsto (x, -\dot{x}, -y, \dot{y})$, yielding the symmetry $f(A\mathbf{x}) = -Af(\mathbf{x})$. So, any orbit that starts on the plane $(x, 0, 0, \dot{y})$ has its backward orbit given by $x(-t) = Ax(t)$. In other words, an orbit that connects the unstable boundary and the plane $(x, 0, 0, \dot{y})$ is a symmetric homoclinic orbit for the critical equilibrium: We do not have to integrate the stable boundary backwards. We show that the unstable manifold has an intersection with $(x, 0, 0, \dot{y})$, and we obtain the homoclinic orbits in Fig. 19 by flipping the orbits along the symmetry axis.

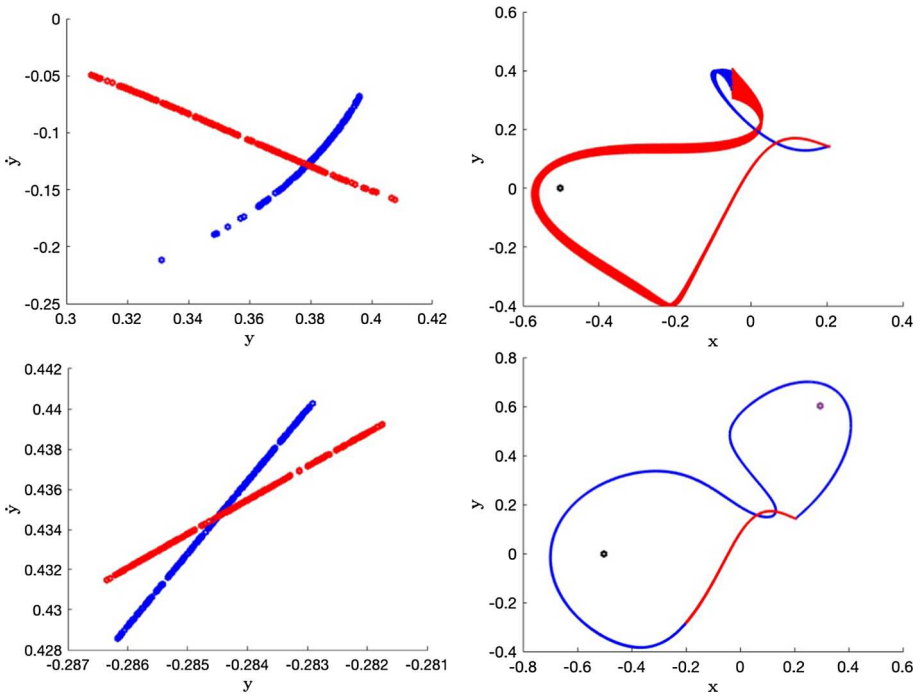

Fig. 18 Numerical integration of the stable and unstable manifold at v_{c_2}**:** We found two "large" homoclinic orbits of L_c by numerically integrating the (un)stable manifold. The red surface is the backward flow of part of the edge of stable manifold, and the blue surface is the forward flow of part of the edge of the unstable manifold. In the top left figure, we plot the intersection of the forward and backward flow and the line $x = -0.05$ with positive x-derivative. As there is a transverse connection in the $(y, \dot{y})$-plane, we find the enclosure of a homoclinic orbit, which is the top right figure. In the bottom left figure, we plot the intersection of the forward and backward flow and the line $x = -0.2$ with positive x-derivative. As there is a transverse connection in the $(y, \dot{y})$-plane, we find the enclosure of a homoclinic orbit, which is the bottom right figure

These results suggest a rich transverse homoclinic orbit structure at $\mathfrak{D}$. Not all of the homoclinic orbits found at the critical curve have shapes reminiscent of the basic triple Copenhagen homoclinics $\gamma_{1,2,3,4,5,6}$. For example, the middle right frame of Fig. 19 illustrates a homoclinic orbit with no apparent analogue in the triple Copenhagen problem.

5 Conclusions

Informed by the numerical explorations discussed in the main text of the paper, we propose the following conjectures concerning the global dynamics of the CRFBP. First, and based on the observation in Remark 1, we conjecture that each of the short triple Copenhagen homoclinic orbits undergoes a type II bifurcation.

Conjecture 1 Any parameter continuation of the triple Copenhagen homoclinic orbits $\gamma_{1,2,3}$ toward the critical curve $\mathfrak{D}$ results in a Belyakov–Devaney bifurcation before the termination of the family.

Recall that when the γ_1 family of homoclinic orbits is continued along one of the three parameter lines $\ell_{1,2,3}(s)$, the numerical continuation breaks down before the critical curve.

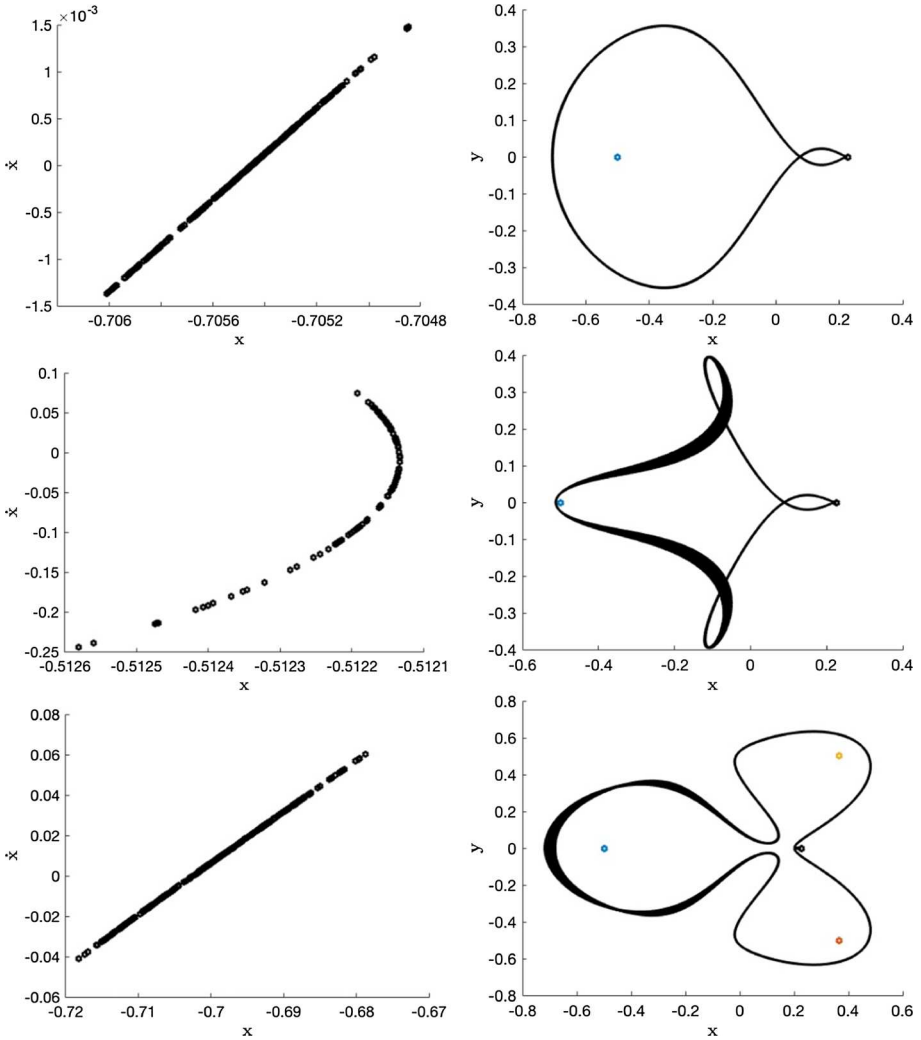

Fig. 19 Numerical integration of the stable and unstable manifold at v_{c_3}**:** We found three "large" homoclinic orbits of L_c by numerically integrating the unstable manifold. In the left figures, we plot the intersection of forward flow of part of the edge of the unstable manifold and the line $y = 0$. In all three figures we see that in the $(x, \dot{x})$-plane we have a transverse intersection with the line $\dot{x} = 0$. Hence, due to symmetry, we obtained a region in which a homoclinic orbit lies. In the right figures we plotted the corresponding region in which a homoclinic orbit lies

The γ_1 family exhibits the least robustness with respect to parameter continuation along these three parameter lines, and we conjecture that this behavior is general.

Conjecture 2 The γ_1 family *never* continues to the critical curve $\mathfrak{D}$.

The γ_2 family, on the other hand, exhibits the most robustness, and we find that we are able to continue along each of the three parameter lines almost until the homoclinic orbits shrink to points. Moreover, we confirmed by considering the normal form that when L_2 is

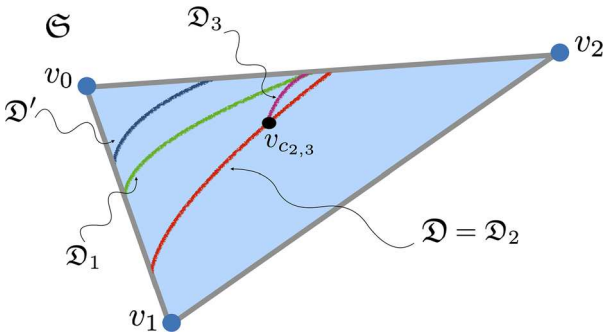

Fig. 20 Conjectured critical curves for the $\gamma_{1,2,3}$ families: conjectured critical lines for the $\gamma_{1,2,3}$ families of homoclinic orbits

close to L_0, there is a short homoclinic orbit for L_0 which winds around L_2. We conjecture that this is the general picture.

Conjecture 3 The γ_2 family *always* continues to the critical curve $\mathfrak{D}$, where it vanishes with L_0 and L_2 in the saddle node bifurcation.

The behavior of the γ_3 family is the most complicated. For parameters on the $m_2 = m_3$ edge of the parameter simplex, the problem has symmetry about the x-axis. Then, the behavior of γ_3 on the $\ell_3(s)$ line mirrors the behavior of γ_1, which breaks down before $\mathfrak{D}$. Similarly, for parameters on the $m_1 = m_2$ edge of the parameter simplex the problem has symmetry about the line through the third primary bisecting the edge of the triangle connecting the first to the second primary. In this case the behavior of γ_3 on the $\ell_1(s)$ line mirrors the behavior γ_2, which continues all the way to $\mathfrak{D}$ where it disappears. Moreover, the normal form calculation suggests that there is a "short" homoclinic around L_3 for parameter values near the pitchfork bifurcation, and our numerics confirm this, with a shape suggestive of the γ_3 family. We conjecture that the discussion above tells the full story.

Conjecture 4 The γ_3 family of homoclinics continues to the critical curve $\mathfrak{D}$ when $m_2 \approx m_3$ and does not reach $\mathfrak{D}$ when $m_1 \approx m_2$. There is a single parameter value on $\mathfrak{D}$ separating these behaviors.

Indeed, we propose a little more. Let $\mathfrak{D}'$ denote the curve in parameter space where the stability of L_0 changes from bi-focus to a saddle with real distinct eigenvalues. Let $\mathfrak{D}_1$ denote the set of points in $\mathfrak{S}$ where the γ_1 family loses transversality and breaks down in a type IV bifurcation. We claim that $\mathfrak{D}_1$ is an analytic simple closed curve from the $m_1 = m_2$ edge to the $m_2 = m_3$ edge which does not intersect $\mathfrak{D}$. Define $\mathfrak{D}_2$ and $\mathfrak{D}_3$ analogously. We claim that $\mathfrak{D}_2 = \mathfrak{D}$ and that $\mathfrak{D}_3$ coincides with $\mathfrak{D}$ near the $m_1 = m_2$ edge, separates at a single parameter value where there is a type V bifurcation, and then intersects with $\mathfrak{D}_1$ only at the $m_2 = m_3$ parameter edge. We conjecture that the separation of $\mathfrak{D}$ and $\mathfrak{D}_3$ occurs at $v_c = (m_1, m_2, m_3) \in \mathfrak{D}$ with $m_1 \in (0.425, 0.426)$. We also claim that $\mathfrak{D}'$ lies entirely to the left of $\mathfrak{D}_1$, so that each of the $\gamma_{1,2,3}$ families undergoes a Belyakov–Devaney bifurcation on $\mathfrak{D}'$. A graphical depiction of the conjectures is given in Fig. 20.

Resolving these conjectures would seem to require substantial additional work. Moreover, since the mathematically rigorous characterization of the equilibrium set given in Leandro (2006), Barros and Leandro (2011), Barros and Leandro (2014) required the use of computer-assisted methods of proof, it seems likely resolution of the conjectures would require similar methods. We remark that one-parameter families of connecting orbits have been studied using

computer-assisted methods of proof, see, for example, van den Berg et al. (2018). Computer-assisted proofs of bifurcations of connecting orbits for maps were studied in Adams and James (2019), and there is reason to believe that these techniques could be extended to differential equations. We further mention that computer-assisted methods of proof have been devised for studying center manifolds (Capiński and Roldán 2011) in celestial mechanics problems. Finally, note that validated numerical methods for infinite dimensional multi-parameter continuation problems have been developed (Gameiro et al. 2016) so that many of the techniques needed for establishing the conjectures above exist. Combining and extending existing methods to resolve the proposed conjectures would represent a substantial leap in the state of the art of computer-assisted methods of proof for global analysis of nonlinear systems.

There exists a substantial literature on numerical methods for studying degenerate connecting orbits. We refer, for example, to works of Oldeman et al. (2003), Doedel et al. (1997), Friedman and Doedel (1993), Beyn (1994), Champneys et al. (1996), Beyn et al. (2002), Champneys and Kuznetsov (1994), Oldeman et al. (2001). Since these works are based on implicit function theory/Newton's method applied to appropriate systems of constraints, it is reasonable to suppose that such methods are amenable to the kind of a-posteriori analysis that underlies the papers discussed in the previous paragraph exploit. In other words, the theoretical framework needed for framing computer-assisted proofs of the critical and degenerate connecting orbits already exists.

Another concrete open question is suggested by the γ_1 family, which appears to always terminates in a type IV global bifurcation. If this is indeed the case, then the γ_1 family must collide with another homoclinic family and disappear at $\mathfrak{D}_1$, begging the question: *What is the other homoclinic family participating in this bifurcation?* Or, if our guess is mistaken and γ_1 does not terminate in a type IV bifurcation so that there is no second family of homoclinics terminating at $\mathfrak{D}_1$, then what is happening there? Put another way, if $\mathfrak{D}_1$ is not a type IV bifurcation curve then what is it? We have not yet begun to explore this very natural question.

Before concluding, we remark that another interesting project would be to generalize the current study to the $\gamma_{4,5,6}$ families. We did not undertake this work for two reasons: First, our work on the $\gamma_{1,2,3}$ family already requires a substantial number of pages to describe. But more importantly, the $\gamma_{4,5,6}$ families do not participate in blue sky catastrophes with any Lyapunov families of periodic orbits. Rather, they are related to certain periodic orbits around the primaries coming from the rotating Kepler problem. This complicates the use of the blue sky tests conducted in Sect. 3. Nevertheless, a follow-up study on the robustness of the $\gamma_{4,5,6}$ families could be an interesting project.

Acknowledgements The authors would like to thank J.B. van den Berg and Bob Rink for many helpful discussions and much encouragement as this work progressed. The authors owe sincere thanks to two anonymous referees who carefully read the submitted version of the manuscript, and made a number of insightful comments and corrections which improved the final printed version of the paper. W. Hetbrij was partially supported by NWO-VICI Grant 639033109. J.D. Mireles James was partially supported by NSF Grant DMS-1813501.

A Numerical continuation of periodic and connecting orbits in conservative systems

Before discussing continuation schemes for two point boundary value problems, we first introduce a little notation, and review some basic concepts from the elementary theory of

differential equations. A comprehensive reference for the material discussed in this section is the book of Chicone (2006).

Suppose that for each $s \in [a, b] \subset \mathbb{R}$ the set Ω_s is an open subset of $\mathbb{R}^d$, and let $f_s : \Omega_s \times [a, b] \to \mathbb{R}^d$ be a one-parameter family of smooth vector fields, depending smoothly on the parameter s. Suppose further that for each $s \in [a, b]$ there is a smooth function $E_s : \Omega_s \to \mathbb{R}$ having that

$$\nabla E_s(\mathbf{x}) \cdot f_s(\mathbf{x}) = 0,$$

for all $\mathbf{x} \in \Omega_s$. It follows that the function E_s is a conserved quantity for the vector field f_s, in the sense that if $\gamma : [0, T] \to \Omega_s$ is a solution of the differential equation

$$\gamma'(t) = f_s(\gamma(t)),$$

then

$$E_s(\gamma(t)) = E_s(\gamma(0)),$$

for all $t \in [0, T]$. To see this, simply differentiate to obtain

$$\begin{aligned} \frac{d}{dt} E_s(\gamma(t)) &= \nabla E_s(\gamma(t)) \cdot \gamma'(t) \\ &= \nabla E_s(\gamma(t)) \cdot f(\gamma(t)) \\ &= 0, \end{aligned}$$

as $\gamma(t) \in \Omega_s$ for $t \in [0, T]$, and E_s is constant on solution curves as desired.

Next we introduce the notion of the flow map generated by f_s. Indeed, suppose that $x_0 \in \Omega_s$. Since f_s is differentiable (and hence locally Lipschitz), there exists a maximal $-\infty \leq \omega_{x_0} < 0 < \tau_{x_0} \leq \infty$ so that the solution of the initial value problem

$$x'(t) = f_s(x(t)), \qquad x(0) = x_0$$

exists and is unique for all $t \in [\omega_{x_0}, \tau_{x_0}]$. We write

$$x(t) = \phi(x_0, t, s),$$

for $t \in [\omega_{x_0}, \tau_{x_0}]$ to denote the local flow map. The map has the property that

$$\phi(x_0, t_1 + t_2) = \phi(\phi(x_0, t_1), t_2),$$

for all $t_1, t_2 \in [\omega_{x_0}, \tau_{x_0}]$ which have that $t_1 + t_2 \in [\omega_{x_0}, \tau_{x_0}]$.

It is a classic theorem of differential equations that ϕ is a smooth function of $s \in (a, b)$, and of $x_0 \in \Omega_s$ and of $t \in (\omega_{x_0}, \tau_{x_0})$, and we would like to compute the partial derivatives. Since $x(t) = \phi(x_0, t, s)$ is a solution curve for the differential equation, we have that

$$\frac{\partial}{\partial t} \phi(x_0, t, s) = f(\phi(x_0, t, s)), \qquad t \in (\omega_{x_0}, \tau_{x_0}). \tag{9}$$

The derivatives with respect to x_0 and s are more involved, but satisfy the so-called *variational equations*. More precisely, let

$$M(t) = D_x \phi(x_0, t, s).$$

Then, $M(t)$ satisfies the non-autonomous, homogeneous, linear matrix differential equation

$$M'(t) = D_x f_s(\phi(x_0, t, s)) M(t), \qquad M(0) = \mathrm{Id},$$

the equation of first variation with respect to initial conditions. Similarly, let

$$\eta(t) = \frac{\partial}{\partial s}\phi(x_0, t, s).$$

Then, $\eta(t)$ satisfies the non-autonomous, inhomogeneous, linear differential equation

$$\eta'(t) = D_x f_s(\phi(x_0, t, s))\eta(t) + \frac{\partial}{\partial s} f_s(\phi(x_0, t, s)) \qquad \eta(0) = 0,$$

the equation of first variation with respect to the parameter s. Of course, if f has other parameters, then partial derivatives of ϕ with respect to these parameters are found the same way.

Suppose now that $s \in [a, b]$ and $x_0 \in \Omega_s$ are fixed and that $0 < \tau \leq \tau_{x_0}$ is a fixed "step size." In practice the quantities $\phi(x_0, \tau, s)$, $M(\tau)$, and $\eta(\tau)$ are computed simultaneously by numerically integrating the system of equations

$$\begin{aligned} x'(t) &= f_s(x(t)) \\ M'(t) &= D_x f_s(x(t))M(t) \\ \eta'(t) &= D_x f_s(x(t))\eta(t) + \tfrac{\partial}{\partial s} f_s(x(t)) \end{aligned} \tag{10}$$

with initial data $x(0) = x_0$, $M(0) = \mathrm{Id}$, and $\eta(0) = 0$ up to time τ. The computations carried out in the present work we exploit the standard "off the shelf" MATLAB integration scheme known as `rk45` to numerically solve these initial value problems when necessary.

A.1 Periodic orbits of conservative systems

In this section we work at a fixed parameter value in $s \in [a, b]$ and hence suppress the dependence of f and ϕ on s all together. So, let $f = f_s : \Omega \to \mathbb{R}^d$ denote our conservative vector field with $\Omega \subset \mathbb{R}^d$ open and $E = E_s : \Omega \to \mathbb{R}$ the conserved quantity.

It is well known (and much exploited in the present work) that periodic orbits of a conservative vector field appear in one parameter "tubes" parameterized by the conserved quantity, or equivalently—by period. See, for example, the discussion of periodic orbits in the book of Meyer and Offin (2017). So, one locally isolates a particular periodic orbit in the "tube" by fixing a target period $T > 0$ as a problem parameter. Let $\tau_1, \ldots, \tau_K > 0$ have that $\tau_1 + \ldots + \tau_K = 1$. A periodic orbit is equivalent to a solution $x_1, \ldots, x_K \in \Omega$ of the system of equations

$$\begin{aligned} \phi(x_1, \tau_1 T) &= x_2 \\ \phi(x_2, \tau_2 T) &= x_3 \\ &\vdots \\ \phi(x_K, \tau_K T) &= x_1. \end{aligned}$$

Our strategy is to solve the system of equations using a Newton method, in which case it is important to consider only systems with isolated zeros. Yet this system of equations cannot have a unique solution, as any phase shift of a periodic orbit is again a periodic orbit. To isolate, we introduce a Poincare phase condition. That is, we require that the periodic orbit crosses a fixed co-dimension one affine subspace (or "plane") $P \subset \mathbb{R}^d$ at time zero. Let $y_0 \in \mathbb{R}^d$ be a point in the desired plane P and $v \in \mathbb{R}^d$ be the direction vector of the plane. Then, $x_1 \in \mathbb{R}^d \in P$ if and only if

$$(x_1 - y_0)^T \cdot v = 0.$$

When we append this equation to the system the resulting augmented system has one more equation than unknowns. The system needs to be balanced by either eliminating an equation (which can be done using the conserved quantity) or by introducing an "unfolding parameter" $\alpha \in \mathbb{R}$—the approach taken in the present work. An unfolding parameter is an artificial variable which balances the system, and which should have the special property that it must be zero at a periodic solution (this will be made precise below).

Deciding how to insert a new parameter into the problem is a delicate question, yet for conservative vector fields there is a canonical choice. We describe the classic approach, as developed in references (Doedel et al. 2003; Muñoz Almaraz et al. 2003), and define the unfolded family of vector fields by

$$f_\alpha(x) = f(x) + \alpha \nabla E(x)^T,$$

where $\alpha \in \mathbb{R}$ is the new unfolding parameter. Suppose now that $\gamma : [0, T] \to \Omega$ is a periodic solution of

$$\gamma'(t) = f_\alpha(\gamma(t)).$$

If $\nabla E(\gamma(t))$ not identically zero on $[0, T]$, then $\alpha = 0$, and—in fact—γ is a period T solution of $\gamma' = f(\gamma)$.

To see this, consider the real-valued function

$$g(t) = E(\gamma(t)).$$

We have that

$$\begin{aligned} g'(t) &= \nabla E(\gamma(t))\gamma'(t) \\ &= \nabla E(\gamma(t)) f_\alpha(\gamma(t)) \\ &= \nabla E(\gamma(t)) f(\gamma(t)) + \alpha \nabla E(\gamma(t)) \nabla E(\gamma(t))^T \\ &= \alpha \|\nabla E(\gamma(t))\|^2, \end{aligned}$$

as f conserves E. Since γ has period T, we have that $\gamma(0) = \gamma(T)$ and hence

$$0 = E(\gamma(T)) - E(\gamma(0)) = g(T) - g(0).$$

But

$$\begin{aligned} g(T) - g(0) &= \alpha \int_0^T \|\nabla E(\gamma(t))\|^2 \, dt \\ &= 0 \end{aligned}$$

if and only if $\alpha = 0$, as $\|\nabla E(\gamma(t))\|$ is not identically zero.

Now, denote by $\phi(x, t, \alpha)$ the local flow generated by f_α, and note that the partial derivative of ϕ with respect to α is computed by solving the equation of first variation with respect to α as discussed in the previous section. Define the map $F : \Omega^K \times \mathbb{R} \subset \mathbb{R}^{dK+1} \to \mathbb{R}^{dK+1}$ by

$$F_T(x_1, x_2, x_3, \ldots, x_{K-1}, x_K, \alpha) = \begin{pmatrix} \phi(x_1, \tau_1 T, \alpha) - x_2 \\ \phi(x_2, \tau_2 T, \alpha) - x_3 \\ \vdots \\ \phi(x_{K-1}, \tau_{K-1} T, \alpha) - x_K \\ \phi(x_K, \tau_K T, \alpha) - x_1 \\ (x_1 - y_0)^T \cdot v \end{pmatrix} \tag{11}$$

and note that a zero of F_T is an orbit of period T for f. Let $\mathbf{x} = (x_1, \ldots, x_K, \alpha) \in \mathbb{R}^{dK+1}$. The number of equations matches the number of unknowns, and the system is amenable to the Newton method

$$\mathbf{x}_{j+1} = \mathbf{x}_j + \Delta_j,$$

where Δ_j is a solution of the linear system

$$DF_T(\mathbf{x}_j)\Delta_j = F_T(\mathbf{x}_j).$$

The derivative involves only partial derivatives of the local flow, which are computed by solving variational equations (10). This is referred to as a *multiple shooting* scheme for the periodic orbit.

Remark 3 Some mechanical systems have the property that $\nabla E(x) = 0$ if and only if $f(x) = 0$. This happens, for example, when f is a Hamiltonian vector field and E is the Hamiltonian. In this case, $\nabla E(\gamma(t))$ is not identically zero if and only if $\gamma(t)$ is not constant, making this non-degeneracy hypothesis especially easy to check. We also remark that for some mechanical systems it is possible to simplify the unfolded vector field f_α. For example, if f is a conservative system derived from Newton's laws, then one gets the same result by adding α times a linear dissipative term to the system rather than using the canonical gradient term. See Muñoz Almaraz et al. (2003).

A.2 Continuation with respect to period in conservative systems

Note that the period $T > 0$ appears as a continuation parameter in the map F_T defined in Eq. (11). Then, supposing that $\mathbf{x}_0$ has $F_T(\mathbf{x}_0) = \mathbf{0}$ and that $DF_T(\mathbf{x}_0)$ is non-singular, we have by the implicit function theorem that there is a smooth branch of solutions of $\mathbf{x}(\beta)$ defined for $\beta \in (T - \epsilon, T + \epsilon)$, with $\mathbf{x}(T) = \mathbf{x}_0$. Moreover, since

$$F_\beta(\mathbf{x}(\beta)) = 0, \qquad \text{for} \beta \in (T - \epsilon, T + \epsilon),$$

we have, after taking the derivative with respect to β, that

$$DF_\beta(\mathbf{x}(\beta))\frac{d}{d\beta}\mathbf{x}(\beta) + \frac{\partial}{\partial\beta}F_\beta(\mathbf{x}(\beta)) = 0.$$

Let $\mathbf{x}'(T) = \mathbf{v}$. Then, $\mathbf{v}$ solves the equation

$$DF_T(\mathbf{x}_0)\mathbf{v} = -\frac{\partial}{\partial\beta}F_T(\mathbf{x}_0),$$

giving the linear approximation of the branch through $\mathbf{x}_0$. We note that the right-hand side consists of terms of the form

$$\frac{\partial}{\partial\beta}\phi(x_j, \tau_j T, \alpha) = \tau_j f_\alpha(\phi(x_j, \tau_j T, \alpha),$$

see Eq. (9). These expressions depend only on the unfolded vector field.

Choosing a $\beta \neq T$, we take

$$\mathbf{x}_1 = \mathbf{x}_0 + (\beta - T)\mathbf{v},$$

as the first-order approximation of $\mathbf{x}(\beta)$, corresponding to the periodic orbit with period $\beta \in (T - \epsilon, T + \epsilon)$ in a nearby energy level. Letting $\mathbf{x}_1$ serve as the initial guess for a zero of F_β, we run Newton's method and converge to a new solution—for $|\beta - T|$ small enough.

The process can be continued until the curve $\mathbf{x}(\beta)$ undergoes a bifurcation. Such bifurcations are indicated by the singularity of the derivative DF_T, and are used to detect interesting phenomena in the main body of the paper. We remark that the appearance of a saddle node bifurcation is not dynamically important in this context, as it indicates only that frequency does not vary monotonically within the "energy tube". The tube itself is the object of interest.

We continue through such saddle node bifurcations using "pseudo-arclength continuation," a small modification of the algorithm just discussed. More complete discussion of numerical algorithms based on pseudo-arclength continuation is found in the book of Kuznetsov (2004). See also Kuznetsov and Meijer (2019), Dhooge et al. (2006), Beyn et al. (2002).

A.3 Homoclinic orbits in conservative systems

Suppose that for $s_0 \in [a, b]$, $p_0 \in \Omega_{s_0}$ is a hyperbolic equilibrium solution of f_{s_0}. Suppose in addition that d_u, d_s are, respectively, the dimension of the unstable/stable eigenspaces and that $d_u + d_s = d$. Since p_0 is a hyperbolic equilibrium solution, there exists an $\delta > 0$ and $p_s : (s_0 - \delta, s_0 + \delta) \to \mathbb{R}^d$ so that $p(0) = p_0$ and

$$f_s(p(s)) = 0 \qquad \text{for all} s \in (s_0 - \delta, s_0 + \delta).$$

Moreover, we can choose $\delta > 0$ so that the dimension of the unstable/stable eigenspaces attached to $p(s)$ is d_u and d_s, respectively, for $s \in (s_0 - \delta, s_0 + \delta)$. Since f_s depends smoothly on $s \in [a, b]$, the parameterizations of the local unstable and stable manifolds depend smoothly on s as well. Let $D_{u,s}$ be, respectively, the unit balls in $\mathbb{R}^{d_{u,s}}$ and suppose that $P_s : D_u \times (s_0 - \delta, s_0 + \delta) \to \mathbb{R}^d$ and $Q_s : D_s \times (s_0 - \delta, s_0 + \delta) \to \mathbb{R}^d$ are smooth parameterizations of the local unstable and stable manifolds attached to $p(s)$. In particular, assume that for $s \in (s_0 - \delta, s_0 + \delta)$, $w \in D_u \subset \mathbb{R}^{d_u}$, and $z \in D_s \subset \mathbb{R}^{d_s}$ we have that

$$\lim_{t \to -\infty} \phi(P(w, s), t, s) = p(s) \qquad \text{and} \qquad \lim_{t \to \infty} \phi(Q(z, s), t, s) = Q(s).$$

Much like the case of a periodic orbit discussed above, we have that an infinitesimal shift of a homoclinic orbit segment is itself a homoclinic orbit segment. Then, a phase condition is required if we want to isolate a solution of the system. We proceeded as follows, and define appropriate sections in the domains of P and Q, respectively. That is, we take $w : [-1, 1]^{d_u - 1} \to D_u$ and $z : [-1, 1]^{d_s - 1} \to D_s$ parameterizations of co-dimension one surfaces in D_u and D_s. We refer to the parameterized surfaces as "phase surfaces" in D_u and D_s, and define

$$\hat{P}(\sigma, s) = P(w(\sigma), s)$$

and

$$\hat{Q}(\theta, s) = Q(z(\theta), s).$$

Let $s \in (s_0 - \delta, s_0 + \delta)$, $K \in \mathbb{N}$ and $\tau_1, \ldots, \tau_K > 0$ have $\tau_1 + \ldots + \tau_K = 1$. We seek $x_1, \ldots, x_K \in \Omega_s$, $\sigma \in [-1, 1]^{d_u - 1}$, $\theta \in [-1, 1]^{d_s - 1}$, and $T > 0$ so that

$$\begin{aligned} \hat{P}(\sigma, s) &= x_1 \\ \phi(x_1, \tau_1 T, s) &= x_2 \\ \phi(x_2, \tau_2 T, s) &= x_3 \\ &\vdots \end{aligned}$$

$$\phi(x_{K-1}, \tau_{K-1}T, s) = x_K$$
$$\phi(x_K, \tau_K T, s) = \hat{Q}(\theta, s).$$

A solution of this system of equations has that each of the points $\hat{P}(\sigma, s)$, $x_1, \ldots, x_K$, and $\hat{Q}(\theta, s)$ lies on the same homoclinic orbit to $p(s)$. That is, the homoclinic orbit is generated by flowing forward or backward any of these points. It is worth noting that $T > 0$ is the "time of flight" from the unstable to the stable phase surface.

Noting that $(\sigma, \theta) \in \mathbb{R}^{d_u+d_s-2} = \mathbb{R}^{d-2}$ and counting variables, we see that $(\sigma, \theta, x_1, \ldots, x_K, T) \in \mathbb{R}^{dK+d-1}$, while the system of equations takes values in $\mathbb{R}^{dK+d}$. Again—and in direct analogy with the situation encountered when discussing periodic orbits—we have one too few unknowns. Just as in the periodic orbit case the system can be balanced by either adding an "unfolding parameter," or by exploiting the conserved quantity to eliminate an equation.

Extending the ideas described in the previous section, we once again employ the classic unfolding parameter technique of Doedel et al. (2003), Muñoz Almaraz et al. (2003), and define

$$f_{s,\alpha}(x) = f_s(x) + \alpha \nabla E_s(x)^T.$$

Let $\phi(x, t, s, \alpha)$ denote the associated flow. Arguing exactly as in the periodic case, we have that if $\gamma : [0, T] \to \mathbb{R}^d$ is an orbit with initial conditions $\gamma(0) = P(\sigma, s)$ and terminal conditions $\gamma(T) = Q(\sigma, s)$, then $\alpha = 0$. This relies on the fact that P and Q parameterize unstable/stable manifolds for the conservative vector field f_s, hence lie in the level set of the equilibrium solution. That is,

$$E_s(P(\theta, s)) = E_s(Q(\sigma, s)) = E_s(P(s)),$$

for all $\sigma \in [-1, 1]^{d_u-1}$, $\theta \in [-1, 1]^{d_s-1}$.

Then, for fixed $s \in (s_0 - \delta, s_0 + \delta)$ a zero of the map $F_s : [-1, 1]^{d_u-1} \times [-1, 1]^{d_s-1} \times \Omega_s^K \times \mathbb{R} \times \mathbb{R} \subset \mathbb{R}^{dK+d} \to \mathbb{R}^{dK+d}$ defined by

$$F_s(\sigma, \theta, x_1, \ldots, x_K, T, \alpha) = \begin{pmatrix} \hat{P}(\sigma, s) - x_1 \\ \phi(x_1, \tau_1 T, s, \alpha) - x_2 \\ \phi(x_2, \tau_2 T, s, \alpha) - x_3 \\ \vdots \\ \phi(x_{K-1}, \tau_{K-1} T, s, \alpha) - x_K \\ \phi(x_K, \tau_K T, s, \alpha) - \hat{Q}(\theta, s) \end{pmatrix}, \tag{12}$$

has $\alpha = 0$ and that the orbit of any of the points $x_1, \ldots, x_K$ is homoclinic for $p(s)$.

Let $\mathbf{x} = (\sigma, \theta, x_1, \ldots, x_K, T, \alpha)$ denote the independent variable for F_s. If $F_s(\mathbf{x}_0) \approx 0$, then we define the Newton sequence

$$\mathbf{x}_{n+1} = \mathbf{x}_n + \Delta_n,$$

where Δ_n is the solution of the linear equation

$$DF_s(\mathbf{x}_n)\Delta_n = -F_s(\mathbf{x}_n).$$

This approach is a multiple shooting scheme for homoclinic orbits in conservative systems. The iteration converges if $\mathbf{x}_0$ is close enough to a homoclinic orbit segment. Again, the derivative of F_s involves derivatives of P, Q, and ϕ where the derivatives of ϕ with respect to x, α are computed by solving variational Eq. (10). The derivative of ϕ with respect to T is as given in Eq. (9), and depends only on the unfolded vector field.

Remark 4 *(Approximating the parameterizations P and Q)* In practice, it is very common to exploit the first-order approximations of P and Q by their eigenspaces, and indeed this is the approach taken in many of the classic references (Doedel and Friedman 1989; Champneys et al. 1996; Friedman and Doedel 1993; Oldeman et al. 2003; Champneys and Kuznetsov 1994; Oldeman et al. 2001; Calleja et al. 2012; Friedman and Doedel 1993). On the other hand, there exist well-developed methods for numerically computing higher-order approximations of P and Q. We exploit such methods in the present work as they (A) provide improved numerical stability/condition numbers in the boundary value problems defining the homoclinic orbits (just as higher-order numerical integration schemes provide improvements over the standard Euler method), and (B) higher-order methods are necessary for the center manifold calculations exploited in the critical calculations. Using higher-order methods throughout represents a more unified approach. For the high-order approximation of P and Q in the present work, we utilize numerical implementations, based on the parameterization method (Cabré et al. 2003a, b, 2005), and developed in Kepley and James (2019), Kepley and James (2019), Kepley and James (2019).

A.4 Continuation of a conservative homoclinic with respect to a parameter

Suppose that $\mathbf{x}_0$ has $F_{s_0}(\mathbf{x}_0) = 0$, and that $DF_{s_0}(\mathbf{x}_0)$ is non-singular. Then, by the implicit function theorem there exists an $\epsilon > 0$ and a smooth branch of zeros $\mathbf{x}(s)$ so that $F_s(\mathbf{x}(s)) = 0$ for $s \in (s_0 - \epsilon, s_0 + \epsilon)$, and $\mathbf{x}(s_0) = \mathbf{x}_0$. Differentiating with respect to s leads to

$$DF_s(\mathbf{x}(s))\frac{\mathrm{d}}{\mathrm{d}s}\mathbf{x}(s) + \frac{\partial}{\partial s}F_s(\mathbf{x}(s)) = 0.$$

Letting $\mathbf{x}'(s_0) = \mathbf{v}$, we see that $\mathbf{v}$ solves the linear equation

$$DF_s(\mathbf{x}_0)\mathbf{v} = -\frac{\partial}{\partial s}F_s(\mathbf{x}_0).$$

Note that the right-hand side consists of partial derivatives of the flow with respect to α, and that these are found by solving variational equations.

For $s \in (s_0 - \epsilon, s_0 + \epsilon)$ with $|s - s_0| \ll 1$, define

$$\mathbf{x}_1 = \mathbf{x}_0 + (s - s_0)\mathbf{v},$$

as the first-order approximation of $\mathbf{x}(s)$ at s_0. Then, $\mathbf{x}_1$ is the first-order approximation of a homoclinic orbit segment to $p(s)$. We take $\mathbf{x}_1$ as our initial guess for a zero of $F_s(\mathbf{x})$ and once again iterate the Newton scheme. Again, this process can be iterated until $\mathbf{x}(s)$ undergoes a bifurcation.

One technical difficulty is that this procedure requires the computations of derivatives of P and Q with respect to the parameter s. If P and Q are found using the parameterization method as discussed in Remark 4, then the partial derivatives with respect to parameter can be computed using the variational equations developed in James (2015). On the other hand, it is also possible to compute the partial derivatives using finite differencing schemes. For example, if we know $P(\sigma, s_0)$ and $P(\sigma, s_1)$, then we have

$$\frac{\partial}{\partial s}P(\sigma, s_0) \approx \frac{P(\sigma, s_1) - P(\sigma, s_0)}{s_1 - s_0}.$$

Since the parameterizations at the new parameter s_1 have to be computed in order to define the map F_{s_1}, this differencing does not incur any additional cost. In the present work, we find that this differencing scheme is sufficient for our purposes.

B Formal series calculation of the center stable/unstable manifolds

The calculations discussed in Sect. 3 provide supporting evidence for the claims made in Sect. 2 in cases when the homoclinic orbits do not shrink in size to zero. In these cases, failure of the numerical continuation algorithms is taken as an indication that the homoclinic orbits undergo a bifurcation. On the other hand, when the connecting orbit shrinks to zero size, the continuation algorithm eventually fails for other reasons: Essentially, it becomes increasingly difficult to distinguish the homoclinic orbit form the equilibrium solution itself. This is the case for the $\gamma_{2,k}(s)$, $k = 1, 2, 3$ and the $\gamma_{3,1}(s)$ homoclinic families, which we conjectured survive all the way to the critical curve $\mathfrak{D}$.

Fortunately, small amplitude homoclinic orbits can be studied by completely different—and much more local—center manifold methods. We now turn to a method for computing the center manifold of a critical libration point when the system has parameter values on (or near) the critical curve $\mathfrak{D}$. We employ a novel parameterization method recently developed by van den Berg, Rink, and the first author (van den Berg et al. 2020).

The parameterization method is a functional analytic framework for studying invariant manifolds developed by Cabré et al. (2003a, b, 2005). We refer the interested reader also to the comprehensive recent book on the subject by Haro et al. (2016). The parameterization method was used extensively in the work of Kepley and James (2019), Kepley and James (2019), and also in the recent work of Murray and the second author on homoclinic dynamics for planar and spatial periodic orbits in the CRTBP (Murray and James 2017, 2020).

Of course, computational methods for center manifolds, and related methods for numerical calculation of normal forms, have a long history in the celestial mechanics literature. Other method than those we choose could have been used here. The literature is substantial, and a thorough review of the literature is beyond the scope of the present work. We refer the interested reader to the works of Simó (1988), Cobos and Simó (1998), Jorba and Masdemont (1999), Jorba (1999), Jorba et al. (1999), Jorba and Villanueva (1998), Canalias et al. (2006), Farrés and Jorba (2010). We also refer to the books (Gómez et al. 2001, a, b, c) for extensive computational treatment of invariant manifolds and their use in space mission design. Much more detail on center manifolds for parabolic equilibria with applications to celestial mechanics is found in Baldomá et al. (2017), Baldomá et al. (2007), Baldomá and Fontich (2004). This interested reader may want to consult the lecture notes (Simo 1990).

Turning to the parameterization method, let us establish some notation. We focus here on the case that the phase space is four-dimensional, as this is the only case encountered in the present work; however, most of the results reported here generalize as discussed in the references above. Let $\Omega \subset \mathbb{R}^4$ be an open subset and suppose that $f : \Omega \to \mathbb{R}^4$ is a smooth and conservative vector field. Consider a connected open set $U \subset \mathbb{R}^d$ with $d = 1, 2, 3$, a one-to-one map $K : U \to \mathbb{R}^4$, and a vector field $r : \mathbb{R}^d \to \mathbb{R}^d$. If K satisfies the infinitesimal invariance equation

$$DK(\mathbf{y})r(\mathbf{y}) = f(K(\mathbf{y})), \qquad \mathbf{y} \in U, \tag{13}$$

then the image of K is locally invariant under the flow generated by f. In fact, K lifts orbits of $\mathbf{y}' = r(\mathbf{y})$ to orbits of f. If the vector field f is inflowing/outflowing on the boundary of $K(U)$, then the image of K is forward/backward invariant. The main idea of the parameterization method is to study appropriate versions of Eq. (13) in various important situations of interest. The geometric meaning of Eq. (13) is illustrated in Fig. 21.

We now describe a version of the parameterization method for parabolic equilibrium solutions. That is, we consider situations where $Df(\mathbf{x}_0)$ has one or more zero eigenvalues.

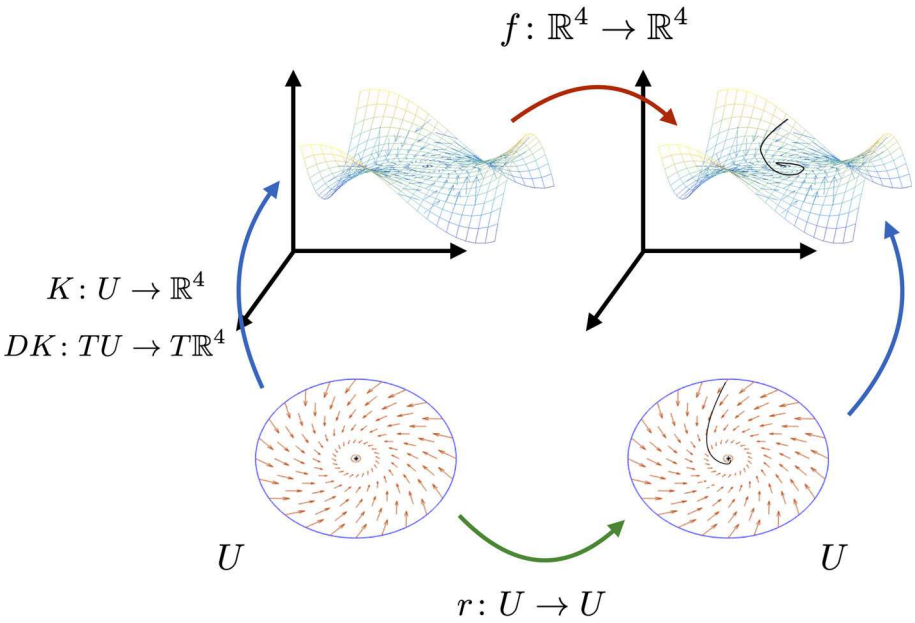

Fig. 21 The geometric meaning of Eq. (13)**:** We are interested in a chart map K parameterizing an invariant manifold patch. The parameterization method singles out special charts satisfying an infinitesimal conjugacy. The idea is that K functions in two complementary ways. On the one hand, K embeds U into the phase space, hence is a chart for a manifold patch. On the other hand, DK maps a vector field r defined in U into the tangent space of this manifold. If the two vector fields—f restricted to the image of K, and the push forward of r by DK are equal (as required by Eq. (13)), then K maps orbits of r to orbits of f and the manifold patch is locally invariant

In the present paper we are primarily interested in the fold bifurcation, though the pitchfork is considered briefly as well.

The technique used here is developed in van den Berg et al. (2020), and has not been applied in the context of celestial mechanics until now. Because of this novelty we discuss the method in somewhat more detail than in the previous two sections, where we reviewed material appearing already in the literature. Returning to Eq. (13), the idea is that we must now solve simultaneously for the embedding K of the center manifold and the model/inner dynamics r.

As seen in Sect. 4, at the saddle-node bifurcation there exists a solution branch which is nonlinear stable, as well as a solution branch which is nonlinear unstable. After we compute the embedding K, we exploit the Jacobi integral E to find those branches. If $h(t)$ is a characterization of the stable solution branch for the conjugate vector field r on the center subspace, we have that $K(h(t))$ is a solution branch of the original differential equation $\dot{\mathbf{x}}(t) = f(\mathbf{x}(t))$ by the construction of K. Thus, the energy E is constant along $K(h(t))$. Furthermore, we have $\lim_{t\to\infty} K(h(t)) = \mathbf{x}_0$; hence,

$$E_0 \stackrel{\text{def}}{=} E(\mathbf{x}_0) = E(\lim_{t\to\infty} K(h(t))) = \lim_{t\to\infty} E(K(h(t))) = E(K(h(t))) \quad \text{for all } t \in \mathbb{R}.$$

If $h(t)$ is a characterization of the unstable branch, we consider the limit of t going to $-\infty$ to again find that

$$E_0 \stackrel{\text{def}}{=} E(\mathbf{x}_0) = E(\lim_{t\to-\infty} K(h(t))) = \lim_{t\to-\infty} E(K(h(t))) = E(K(h(t))) \quad \text{for all } t \in \mathbb{R}.$$

Hence, the (un)stable branch is found by solving the energy equation

$$E \circ K \circ h - E_0 = 0, \tag{14}$$

using a power matching scheme.

B.1 Center stable/unstable manifolds

After finding the stable and unstable branches in the center manifold, we want to construct the center (un)stable manifolds. For convenience, we consider only the center stable manifold in the following sections. The center unstable manifold is similar. We consider connected open sets $X_c \subset \mathbb{R}^2$ and $X_{cs} \subset \mathbb{R}^3$ for the role of U in the invariance Eq. (13) for the center manifold and center stable manifold, respectively. So, for the center stable manifold we seek a solution of the conjugacy equation

$$DK_{cs}(\mathbf{y}, z)r'(x, y, z) = f \circ K_{cs}(x, y, z) \qquad \text{for all } (x, y, z) \in X_{cs}.$$

We know again from van den Berg et al. (2020) that such a conjugacy and conjugate dynamical system exists. In this case, the conjugacy K_{cs} is between the center stable subspace and the center stable manifold, and the vector field r' is the conjugate vector field on the center stable manifold. The center subspace and manifold are naturally embedded in the center stable subspace and manifold, respectively. Hence, we require that $K_{cs}(\mathbf{y}, 0) = K(\mathbf{y})$ for all $\mathbf{y} = (x, y) \in X_c$. It is too much to ask that the conjugate dynamics on the center stable subspace are uncoupled, i.e., $r'(\mathbf{y}, z) = (r(\mathbf{y}), q_s(z))$ cannot hold to all orders. Instead, as we will see in Lemma B.3, we impose that the conjugate vector field in the center direction is uncoupled and the vector field on the stable fibers is given by $q_s(x)z$, where x is the first coordinate on the center subspace, up to arbitrary order. Consider then the conjugacy equation

$$DK_{cs}(\mathbf{y}, z)(r(\mathbf{y}), q_s(x)z) = f \circ K_{cs}(\mathbf{y}, z) \qquad \text{for all } (\mathbf{y}, z) \in X_{cs} \text{ and } \mathbf{y} = (x, y), \tag{15}$$

subject to the constraint $K_{cs}(\mathbf{y}, 0) = K(\mathbf{y})$.

B.2 Formal series calculations

Since center manifolds are in general not analytic, we search for solutions in the space of C^n. Nevertheless, we use formal power series for computational convenience. For notational convenience, we apply a translation and coordinate transformation to move L_c to the origin and have $Df(L_c)$ in Jordan normal form. To find the solution branches $h(t)$, we will need to know the explicit coordinate transformation. In Proposition 1 we found the eigenvectors $\mathbf{v}_0$ and $\mathbf{v}_1$ of the center subspace. The stable and unstable eigenvectors are given by

$$\mathbf{v}_\pm \overset{\text{def}}{=} \left(\Omega_{xy} + 2\lambda_\pm, \lambda_\pm\left(\Omega_{xy} + 2\lambda_\pm\right), \Omega_{yy} - 4, \lambda_\pm\left(\Omega_{yy} - 4\right)\right),$$

where $\lambda_\pm \overset{\text{def}}{=} \mp\sqrt{-4 + \Omega_{xx} + \Omega_{yy}}$ are the stable and unstable eigenvalues. We define the coordinate transformation $\mathcal{C} \overset{\text{def}}{=} (\mathbf{v}_0, \mathbf{v}_1, \mathbf{v}_+, \mathbf{v}_-)$, and redefine $f(\mathbf{x}) \overset{\text{def}}{=} \mathcal{C}^{-1} f(\mathcal{C}\mathbf{x} + \mathbf{x}_0)$.

Lemma B.1 *For every formal series $K_c : \mathbb{R}^2 \to \mathbb{R}^2$ given by*

$$K_c\begin{pmatrix} x \\ y \end{pmatrix} \overset{\text{def}}{=} \begin{pmatrix} x \\ y \end{pmatrix} + \sum_{n=2}^{\infty} \sum_{\substack{(i,j)\in\mathbb{N}^2 \\ i+j=n}} \begin{pmatrix} a_{i,j}x^i y^j \\ b_{i,j}x^i y^i \end{pmatrix}, \tag{16}$$

there exist formal series $K_h : \mathbb{R}^2 \to \mathbb{R}^2$ *and* $r : \mathbb{R}^2 \to \mathbb{R}^2$ *given by*

$$K_h \begin{pmatrix} x \\ y \end{pmatrix} \overset{\text{def}}{=} \sum_{n=2}^{\infty} \sum_{\substack{(i,j)\in\mathbb{N}^2 \\ i+j=n}} \begin{pmatrix} \alpha_{i,j} x^i y^j \\ \beta_{i,j} x^i y^i \end{pmatrix}, \tag{17}$$

$$r \begin{pmatrix} x \\ y \end{pmatrix} \overset{\text{def}}{=} \begin{pmatrix} y \\ 0 \end{pmatrix} + \sum_{n=2}^{\infty} \sum_{\substack{(i,j)\in\mathbb{N}^2 \\ i+j=n}} \begin{pmatrix} \gamma_{i,j} x^i y^j \\ \varepsilon_{i,j} x^i y^i \end{pmatrix}, \tag{18}$$

such that $K \overset{\text{def}}{=} (K_c, K_h)$ *and* r *solve Eq.* (13)*. Furthermore, instead of fixing the constants* $(b_{i,j})_{(i,j)\in\mathbb{N}^2}$ *and solving for the constants* $(\gamma_{i,j})_{(i,j)\in\mathbb{N}^2}$ *among others, we could fix the constants* $(\gamma_{i,j})_{(i,j)\in\mathbb{N}^2}$ *and solve for* $(b_{i,j})_{(i,j)\in\mathbb{N}^2}$*.*

Proof We define the homogeneous polynomials

$$P^n_{K_c} \begin{pmatrix} x \\ y \end{pmatrix} \overset{\text{def}}{=} \sum_{\substack{(i,j)\in\mathbb{N}^2 \\ i+j=n}} \begin{pmatrix} a_{i,j} x^i y^j \\ b_{i,j} x^i y^i \end{pmatrix},$$

$$P^n_{K_h} \begin{pmatrix} x \\ y \end{pmatrix} \overset{\text{def}}{=} \sum_{\substack{(i,j)\in\mathbb{N}^2 \\ i+j=n}} \begin{pmatrix} \alpha_{i,j} x^i y^j \\ \beta_{i,j} x^i y^i \end{pmatrix},$$

$$P^n_{r} \begin{pmatrix} x \\ y \end{pmatrix} \overset{\text{def}}{=} \sum_{\substack{(i,j)\in\mathbb{N}^2 \\ i+j=n}} \begin{pmatrix} \gamma_{i,j} x^i y^j \\ \varepsilon_{i,j} x^i y^i \end{pmatrix},$$

and we will prove that we can recursively define $P^n_{K_h}$ and P^n_r in terms of $P^m_{K_c}$, $P^m_{K_h}$, and P^m_r for $m < n$. It is clear that K_h and r satisfy Eq. (13) up to first order. Now, assume that $P^m_{K_h}$ and P^m_r for $m < n$ are such that K and r satisfy Eq. (13) up to order $n-1$. Then, the n-th-order terms of the difference between the right- and left-hand side of Eq. (13) are given by

$$\begin{aligned} &\sum_{\substack{(i,j)\in\mathbb{N}^2 \\ i+j=n}} \begin{pmatrix} b_{i,j} x^i y^j - \gamma_{i,j} x^i y^j - i a_{i,j} x^{i-1} y^{j+1} \\ -\varepsilon_{i,j} x^i y^j - i b_{i,j} x^{i-1} y^{j+1} \\ \lambda_+ \alpha_{i,j} x^i y^j - i \alpha_{i,j} x^{i-1} y^{j+1} \\ \lambda_- \beta_{i,j} x^i y^j - i \beta_{i,j} x^{i-1} y^{j+1} \end{pmatrix} - \mathcal{P}^n \begin{pmatrix} x \\ y \end{pmatrix} \\ &= \begin{pmatrix} (b_{n,0} - \gamma_{n,0}) x^n \\ -\varepsilon_{n,0} x^n \\ \lambda_+ \alpha_{n,0} x^n \\ \lambda_- \beta_{n,0} x^n \end{pmatrix} + \sum_{\substack{(i,j)\in\mathbb{N}^2 \\ i+j=n \\ (i,j)\neq(n,0)}} \begin{pmatrix} (b_{i,j} - \gamma_{i,j} - (i+1) a_{i+1,j-1}) x^i y^j \\ (-\varepsilon_{i,j} - (i+1) b_{i+1,j-1}) x^i y^j \\ (\lambda_+ \alpha_{i,j} - (i+1) \alpha_{i+1,j-1}) x^i y^j \\ (\lambda_- \beta_{i,j} - (i+1) \beta_{i+1,j-1}) x^i y^j \end{pmatrix} - \mathcal{P}^n \begin{pmatrix} x \\ y \end{pmatrix}. \end{aligned} \tag{19}$$

Here $\mathcal{P}^n$ consists of the n-th-order terms of $f(K^{<n}(\mathbf{y})) - DK^{<n}(\mathbf{y}) r^{<n}(\mathbf{y})$ where $K^{<n} = \sum_{m=1}^{n-1} \left(P^m_{K_c}, P^m_{K_h} \right)$ and $r^{<n} = \sum_{m=1}^{n-1} P^m_r$. For part of the computational implementation of obtaining $\mathcal{P}^n$, we refer to Appendix C. In particular, $\mathcal{P}^n$ is an expression in terms of the constants $a_{i,j}$, $b_{i,j}$, $\alpha_{i,j}$, $\beta_{i,j}$, $\gamma_{i,j}$ and $\varepsilon_{i,j}$ for $i + j < n$. Hence, we find unique $\alpha_{i,j}$, $\beta_{i,j}$, $\gamma_{i,j}$ and $\varepsilon_{i,j}$ such that (19) vanishes starting from $(i, j) = (n, 0)$. In particular, we see that if $\gamma_{i,j}$ is fixed instead of $b_{i,j}$, we can make (19) vanish for $\alpha_{i,j}$, $\beta_{i,j}$, $b_{i,j}$ and $\varepsilon_{i,j}$ instead. □

Now that we have a solution to Eq. (13) and we want to find the stable branch in the center subspace. Recall that we have applied the coordinate transformation

$$\mathcal{C} = \begin{pmatrix} \Omega_{yy} & \Omega_{xy} & \\ 0 & \Omega_{yy} & \\ -\Omega_{xy} & 2-\Omega_{xx} & \mathbf{v}_+ \ \mathbf{v}_- \\ 0 & -\Omega_{xy} & \end{pmatrix},$$

and a translation by $\mathbf{x}_0$ on f. Hence, the conserved quantity becomes $\mathcal{E} = E(\mathcal{C}\mathbf{x} + \mathbf{x}_0)$, with the Jacobi integral $E(x, \dot{x}, y, \dot{y}) = -\left(\dot{x}^2 + \dot{y}^2\right) + 2\Omega(x, y)$.

Lemma B.2 *There exists a formal series $h : \mathbb{R} \to \mathbb{R}^2$ given by*

$$h(t) \overset{\text{def}}{=} \begin{pmatrix} 0 \\ t^3 \end{pmatrix} + \sum_{n=2}^{\infty} \begin{pmatrix} c_n t^n \\ 0 \end{pmatrix} \tag{20}$$

which solves Eq. (14) *if the constant*

$$\mathscr{E} \overset{\text{def}}{=} \Omega_{xxx}\Omega_{yy}^3 - 3\Omega_{xxy}\Omega_{yy}^2\Omega_{xy} + 3\Omega_{xyy}\Omega_{yy}\Omega_{xy}^2 - \Omega_{yyy}\Omega_{xy}^3$$

is nonzero.

Proof We first note that

$$\mathcal{E}_0 \overset{\text{def}}{=} \mathcal{E}(\mathbf{0}) = \mathcal{E}(K(\mathbf{0})) = \mathcal{E}(K(h(0))) = \mathcal{E} \circ K \circ h(0);$$

thus, the constant term of Eq. (14) vanishes. For the higher-order terms we want to find the Taylor expansion of $\mathcal{E}$. Since both Ω_x and Ω_y vanish, we see that $\mathcal{E}$ has no linear terms in its Taylor expansion. We assume that $h(t) = (O(t^2), t^3)$; hence, we have $K(h(t)) = (O(t^2), O(t^3), O(t^4), O(t^4))$. Thus, we must show that the coefficient of $\mathbf{x}_1^2$ in the expansion of $\mathcal{E}$ is 0. We have by the chain rule, we write $\mathcal{E}_{i_1,\ldots,i_m}$ to denote the partial derivative of $\mathcal{E}$ with respect to $x_{i_1},\ldots, x_{i_m}$,

$$\mathcal{E}_{1,1} = 2\Omega_{xx}\Omega_{yy}^2 + 4\Omega_{xy}\Omega_{yy}\left(-\Omega_{xy}\right) + 2\Omega_{yy}\left(-\Omega_{xy}\right)^2 = 0.$$

Therefore, the expansion of $\mathcal{E} \circ K \circ h - \mathcal{E}_0$ is at least of order 5. To rule out terms of order 5, we must show that the coefficient of $\mathbf{x}_1\mathbf{x}_2$ in the expansion of $\mathcal{E}$ is 0. In fact, we have the more general result

$$\mathcal{E}_{1,i} = 2\Omega_{xx}\Omega_{yy}\mathcal{C}_{1,i} + 2\Omega_{xy}\left(\Omega_{yy}\mathcal{C}_{3,i} - \Omega_{xy}\mathcal{C}_{1,i}\right) + 2\Omega_{yy}\left(-\Omega_{xy}\right)\mathcal{C}_{3,i} = 0,$$

for $i = 2, 3, 4$. Thus, the leading term of $\mathcal{E} \circ K \circ h - \mathcal{E}_0$ is of order 6, and its coefficient is determined by the coefficients of $\mathbf{x}_2^2$ and $\mathbf{x}_1^3$ in the expansion of $\mathcal{E}$. We have

$$\begin{aligned} \mathcal{E}_{2,2} &= 2\Omega_{xx}\Omega_{xy}^2 + 4\Omega_{xy}\Omega_{xy}\left(2-\Omega_{xx}\right) + 2\Omega_{yy}\left(2-\Omega_{xx}\right)^2 - 2\left(\Omega_{yy}^2 + \left(-\Omega_{xy}\right)^2\right) \\ &= 2\Omega_{yy}\left(4 - \Omega_{xx} - \Omega_{yy}\right), \\ \mathcal{E}_{1,1,1} &= 2\left(\Omega_{xxx}\Omega_{yy}^3 - 3\Omega_{xxy}\Omega_{yy}^2\Omega_{xy} + 3\Omega_{xyy}\Omega_{yy}\Omega_{xy}^2 - \Omega_{yyy}\Omega_{xy}^3\right). \end{aligned}$$

From the proof of Proposition 1, it follows that both Ω_{yy} and $4 - \Omega_{xx} - \Omega_{yy}$ are nonzero, hence $\mathcal{E}_{2,2} \neq 0$. By assumption, $\frac{1}{2}\mathcal{E}_{1,1,1} = \mathscr{E} \neq 0$. Hence, the leading order of the expansion of $\mathcal{E} \circ K \circ h - \mathcal{E}_0$ is

$$\frac{1}{2}\mathcal{E}_{2,2}t^6 + \frac{1}{6}\mathcal{E}_{1,1,1}c_2^3 t^6.$$

Since we want that $\mathcal{E}\circ K\circ h-\mathcal{E}_0=0$, we must have $\frac{1}{2}\mathcal{E}_{2,2}+\frac{1}{6}\mathcal{E}_{1,1,1}c_2^3=0$, which uniquely determines $c_2=\sqrt[3]{-3\mathcal{E}_{2,2}/\mathcal{E}_{1,1,1}}\neq 0$, with the convention $\sqrt[3]{-x}=-\sqrt[3]{x}$ for $x\geq 0$. We can now recursively find c_n for $n\geq 3$. If we have found c_m for $m\leq n$ such that $\mathcal{E}\circ K\circ h-\mathcal{E}_0$ vanishes for all order up to t^{n+4}, the $n+5$-th order is given by

$$\frac{1}{2}\mathcal{E}_{1,1,1}c_2^2c_{n+1}t^{n+5}+\mathcal{P}_{n+5}.$$

Here $\mathcal{P}_{n+5}$ is the $n+5$-th order term of $\mathcal{E}(K(h^{<n}(t)))-\mathcal{E}_0$ where $h^{<n}(t)=\begin{pmatrix}0\\ t^3\end{pmatrix}+\sum_{m=2}^{n-1}\begin{pmatrix}c_m t^m\\ 0\end{pmatrix}$. Hence, $\mathcal{P}_{n+5}$ only depends c_m for $m\leq n$. Hence, c_{n+1} is uniquely determined and $\mathcal{E}\circ K\circ h-\mathcal{E}_0$ vanishes for all order up to t^{n+5}. Thus, $h:\mathbb{R}\to\mathbb{R}^2$ solves Eq. (14). □

Depending on the sign of t, $h(t)$ is part of the unstable or stable solution branch. We will see that the stable branch is given by $h_s\overset{\text{def}}{=}h|_{t>0}$ and the unstable branch is $h_u\overset{\text{def}}{=}h|_{t<0}$. Finally, we show that we can find a unique expansion for the center stable manifold.

Lemma B.3 *There exists formal series $K_{cs}:\mathbb{R}^3\to\mathbb{R}^4$ and $q_s:\mathbb{R}\to\mathbb{R}$ given by*

$$K_{cs}\begin{pmatrix}x\\ y\\ z\end{pmatrix}=\begin{pmatrix}x\\ y\\ z\\ 0\end{pmatrix}+\sum_{n=2}\sum_{\substack{(i,j,k)\in\mathbb{N}^3\\ i+j+k=n}}\begin{pmatrix}a_{i,j,k}x^iy^jz^k\\ b_{i,j,k}x^iy^jz^k\\ \alpha_{i,j,k}x^iy^jz^k\\ \beta_{i,j,k}x^iy^jz^k\end{pmatrix},\tag{21}$$

$$q_s(x)=\lambda_+ +\sum_{n=2}^{\infty}\zeta_n x^{n-1},\tag{22}$$

which solve Eq. (15). Furthermore, we demand that $a_{i,j,0}$, $b_{i,j,0}$, $\alpha_{i,j,0}$ and $\beta_{i,j,0}$ are given by the constants $a_{i,j}$, $b_{i,j}$, $\alpha_{i,j}$ and $\beta_{i,j}$ from Lemma B.1, respectively. This uniquely determines K_{cs} and q_s except for $\alpha_{0,k-1,1}$ for $k\geq 1$.

Proof We define the homogeneous polynomial

$$\mathcal{P}^n_{K_{cs}}\begin{pmatrix}x\\ y\\ z\end{pmatrix}\overset{\text{def}}{=}\begin{pmatrix}\mathcal{P}^n_{K_c}\\ \mathcal{P}^n_{K_h}\end{pmatrix}\begin{pmatrix}x\\ y\end{pmatrix}+\sum_{\substack{(i,j,k)\in\mathbb{N}^3\\ k\neq 0\\ i+j+k=n}}\begin{pmatrix}a_{i,j,k}x^iy^jz^k\\ b_{i,j,k}x^iy^jz^k\\ \alpha_{i,j,k}x^iy^jz^k\\ \beta_{i,j,k}x^iy^jz^k\end{pmatrix},$$

with $\mathcal{P}^n_{K_c}$ and $\mathcal{P}^n_{K_h}$ defined in Lemma B.1. We want to recursively find $\mathcal{P}^n_{K_{cs}}$ together with ζ_n. Thus, suppose we have found $\mathcal{P}^m_{K_{cs}}$ together with ζ_m for $m\leq n-1$ such that Eq. (15) vanishes up order $n-1$. Then, the n-th order of Eq. (15) is given by

$$\sum_{\substack{(i,j,k)\in\mathbb{N}^3\\ i+j+k=n}}\begin{pmatrix}b_{i,j,k}x^iy^jz^k-\gamma_{i,j}\delta_{k,0}x^iy^j-ia_{i,j,k}x^{i-1}y^{j+1}z^k-k\lambda_+a_{i,j,k}x^iy^jz^k\\ -\varepsilon_{i,j}\delta_{k,0}x^iy^j-ib_{i,j,k}x^{i-1}y^{j+1}z^k-k\lambda_+b_{i,j,k}x^iy^jz^k\\ \lambda_+\alpha_{i,j,k}x^iy^jz^k-\delta_{j,0}\delta_{k,1}\zeta_nx^{n-1}z-i\alpha_{i,j,k}x^{i-1}y^{j+1}z^k-k\lambda_+\alpha_{i,j,k}x^iy^jz^k\\ \lambda_-\beta_{i,j,k}x^iy^jz^k-i\beta_{i,j,k}x^{i-1}y^{j+1}z^k-k\lambda_+\beta_{i,j,k}x^iy^jz^k\end{pmatrix}-\mathcal{P}^n\begin{pmatrix}x\\ y\\ z\end{pmatrix}.\tag{23}$$

Here $\mathcal{P}^n$ consists of the n-th-order terms of $f(K_{cs}^{<n}(\mathbf{y},z))-DK_{cs}^{<n}(\mathbf{y},z)\left(r(\mathbf{y}),q_s^{<n}(x)z\right)$ where $K_{cs}^{<n}=\sum_{m=1}^{n-1}P^m_{K_{cs}}$ and $q_s^{<n}(x)=\lambda_+ +\sum_{m=2}^{n-1}\zeta_m x^{m-1}$. For part of the computational

implementation of obtaining $\mathcal{P}^n$, we refer to Appendix C. Hence, $\mathcal{P}^n$ depends on $\mathcal{P}^m_{K_{cs}}$ and ζ_m for $m < n$. We will show that we can recursively make (23) vanish, starting from $k = 0$ up to $k = n$.

When $k = 0$, (23) reduces to

$$\sum_{\substack{(i,j)\in\mathbb{N}^2\\ i+j=n}} \begin{pmatrix} b_{i,j,0}x^i y^j - \gamma_{i,j}x^i y^j - ia_{i,j,0}x^{i-1}y^{j+1} \\ -\varepsilon_{i,j}x^i y^j - ib_{i,j,0}x^{i-1}y^{j+1} \\ \lambda_+\alpha_{i,j,0}x^i y^j - i\alpha_{i,j,0}x^{i-1}y^{j+1} \\ \lambda_-\beta_{i,j,0}x^i y^j - i\beta_{i,j,0}x^{i-1}y^{j+1} \end{pmatrix} - \mathcal{P}^n \begin{pmatrix} x \\ y \\ 0 \end{pmatrix}. \tag{24}$$

We can show that $\mathcal{P}^n(x, y, 0)$ and $\mathcal{P}^n(x, y)$ from (19) coincide as we assumed that $a_{i,j,0}$, $b_{i,j,0}$, $\alpha_{i,j,0}$, and $\beta_{i,j,0}$ coincide with $a_{i,j}$, $b_{i,j}$, $\alpha_{i,j}$, and $\beta_{i,j}$ for $i + j < n$. Hence, (19) and (24) coincide, and thus demanding $a_{i,j,0} = a_{i,j}, b_{i,j,0} = b_{i,j}, \alpha_{i,j,0} = \alpha_{i,j}$, and $\beta_{i,j,0} = \beta_{i,j}$ ensures that (24) vanishes.

When $k = 1$, (23) reduces to

$$\sum_{\substack{(i,j)\in\mathbb{N}^2\\ i+j=n-1}} z \begin{pmatrix} b_{i,j,1}x^i y^j - ia_{i,j,1}x^{i-1}y^{j+1} - \lambda_+ a_{i,j,1}x^i y^j \\ -ib_{i,j,1}x^{i-1}y^{j+1} - \lambda_+ b_{i,j,1}x^i y^j \\ -\delta_{j,0}\zeta_n x^{n-1} - i\alpha_{i,j,1}x^{i-1}y^{j+1} \\ 2\lambda_-\beta_{i,j,1}x^i y^j - i\beta_{i,j,1}x^{i-1}y^{j+1} \end{pmatrix} - \mathcal{P}^{n,1} \begin{pmatrix} x \\ y \\ z \end{pmatrix}. \tag{25}$$

Here we used in the fourth coordinate that $\lambda_+ = -\lambda_-$. The polynomial $\mathcal{P}^{n,1}$ consists of the terms linear in z in $\mathcal{P}^n$. We can find unique $b_{i,j,1}$, $a_{i,j,1}$, ζ_n, $\alpha_{i,j,1}$, $\beta_{i,j,1}$ such that (25) vanishes. To do so, we first find $b_{n-1,0,1}$, which determines $b_{i,j,1}$ and $a_{i,j,1}$ for $i + j = n - 1$. Secondly, we find ζ_n and $\alpha_{i,j,1}$ independently of each other. Finally, we find $\beta_{n-1,0,1}$ which determines $\beta_{i,j,1}$ for $i + j = n - 1$.

When $k \geq 2$, (23) reduces to

$$\sum_{\substack{(i,j)\in\mathbb{N}^2\\ i+j=n-k}} z^k \begin{pmatrix} b_{i,j,k}x^i y^j - ia_{i,j,k}x^{i-1}y^{j+1} - k\lambda_+ a_{i,j,k}x^i y^j \\ -ib_{i,j,k}x^{i-1}y^{j+1} - k\lambda_+ b_{i,j,k}x^i y^j \\ (1-k)\lambda_+\alpha_{i,j,k}x^i y^j - i\alpha_{i,j,k}x^{i-1}y^{j+1} \\ (k+1)\lambda_-\beta_{i,j,k}x^i y^j - i\beta_{i,j,k}x^{i-1}y^{j+1} \end{pmatrix} - \mathcal{P}^{n,k} \begin{pmatrix} x \\ y \\ z \end{pmatrix}. \tag{26}$$

We again used that $\lambda_+ = \lambda_-$, and the polynomial $\mathcal{P}^{n,k}$ consists of the terms which are of order z^k in $\mathcal{P}^n$. Similar to what we did for (25), we can make (26) vanish. The only difference is that we first find $\alpha_{n-k,0,k}$ instead of ζ_n, and that this uniquely determines $\alpha_{i,j,k}$.

Thus, we can recursively make (23) vanish, and we see that only $\alpha_{0,n-1,1}$ is not uniquely determined. □

C Numerical calculation of the center manifold

In Lemmas B.1 to B.3 we show that there exists formal series for the center manifold, a stable branch on the center manifold, and the center-stable manifold. To compute, for example, the center manifold, we have to calculate some homogeneous polynomials $\mathcal{P}^n(x, y)$. In this case, $\mathcal{P}^n(x, y)$ is the homogeneous polynomial of degree n of the expression $f \circ K^{<n} - DK^{n<} \cdot r^{<n}$, where $K^{<n}$ and $r^{<n}$ are the Taylor polynomial up to order $n - 1$ of K and r, respectively. If we also replace f by its Taylor polynomials, we have to find the homogeneous polynomials of degree n in the expressions $(K^{<n})^\alpha$ and $(r^{<n})^\alpha$ for $|\alpha|_1 \leq n$.

In Haro et al. (2016), radial derivatives are used to find expressions for those homogeneous polynomials, provided that their constant term is nonzero. However, we constructed K and r

in such a way that their constant terms vanish. We can still use the described method to find an expression for g^N in the case that $g(\mathbf{0})$ does vanish. Here g is a multivariate polynomial, which consists of the homogeneous polynomials g_j, and N is a scalar. Let $\mathcal{R}$ denote the radial derivative of g, that is $\mathcal{R}(g)(\mathbf{x}) \stackrel{\text{def}}{=} Dg(\mathbf{x}) \cdot \mathbf{x}$. Then, we find

$$\mathcal{R}(g^N)(\mathbf{x}) = \sum_i \frac{\partial}{\partial x_i} g^N(\mathbf{x}) \cdot x_i = N g^{N-1}(\mathbf{x}) \mathcal{R}(g)(\mathbf{x}).$$

Let $h = g^N$, then we find $g\mathcal{R}(h) = Nh\mathcal{R}(g)$. Since $\mathcal{R}(P) = mP$ for homogeneous polynomials of degree m, we find that the m-th-order term of $g\mathcal{R}(h) - Nh\mathcal{R}(g)$ is given by

$$\sum_{j=0}^{m} ((m-j) - Nj)\, g_j h_{m-j}.$$

Since g_0 vanishes, the first nonzero term of h is $h_N \stackrel{\text{def}}{=} g_1^N$, and for higher-order terms we have the recurrence relation

$$g_1 h_m = \frac{1}{N-m} \sum_{j=2}^{m+1-N} g_j h_{m+1-j}(m+1-j-Nj).$$

We use this to find homogeneous terms of order N in compositions $g_1 \circ g_2$, by replacing g_1 with its Taylor polynomial of order N, and finding the homogeneous terms of $g_1^i(g_2)$ for $1 \leq i \leq N$ using the previous recurrence relation.

References

Adams, R., James, J.D.M.: Validated numerics for continuation and bifurcation of connecting orbits of maps. Qual. Theory Dyn. Syst. **18**(1), 107–137 (2019)

Álvarez-Ramírez, M., Vidal, C.: Dynamical aspects of an equilateral restricted four-body problem. Math. Probl. Eng., pages Art. ID 181360, 23 (2009)

Alvarez-Ramírez, M., Barrabés, E.: Transport orbits in an equilateral restricted four-body problem. Celest. Mech. Dynam. Astronom. **121**(2), 191–210 (2015)

Alvarez-Ramírez, M., Delgado, J., Vidal, C.: Global regularization of a restricted four-body problem. Int. J. Bifur. Chaos Appl. Sci. Engrg. **24**(7), 1450092 (2014)

Alvarez-Ramírez, M., Garcá, A., Palacián, J.F., Yanguas, P.: Oscillatory motions in restricted n-body problems. J. Differ. Equ. **265**, 779–803 (2018)

Baldomá, I., Fontich, E.: Stable manifolds associated to fixed points with linear part equal to identity. J. Differ. Equ. **197**(1), 45–72 (2004)

Baldomá, I., Fontich, E., de la Llave, R., Martín, P.: The parameterization method for one-dimensional invariant manifolds of higher dimensional parabolic fixed points. Discrete Contin. Dyn. Syst. **17**(4), 835–865 (2007)

Baldomá, I., Fontich, E., Martín, P.: Gevrey estimates for one dimensional parabolic invariant manifolds of non-hyperbolic fixed points. Discrete Contin. Dyn. Syst. **37**(8), 4159–4190 (2017)

Baltagiannis, A.N., Papadakis, K.E.: Families of periodic orbits in the restricted four-body problem. Astrophys. Space Sci. **336**, 357–367 (2011)

Baltagiannis, A.N., Papadakis, K.E.: Equilibrium points and their stability in the restricted four-body problem. Int. J. Bifur. Chaos Appl. Sci. Engrg. **21**(8), 2179–2193 (2011)

Barros, J.F., Leandro, E.S.G.: The set of degenerate central configurations in the planar restricted four-body problem. SIAM J. Math. Anal. **43**(2), 634–661 (2011)

Barros, J.F., Leandro, E.S.G.: Bifurcations and enumeration of classes of relative equilibria in the planar restricted four-body problem. SIAM J. Math. Anal. **46**(2), 1185–1203 (2014)

Beyn, W.-J.: Numerical analysis of homoclinic orbits emanating from a Takens-Bogdanov point. IMA J. Numer. Anal. **14**(3), 381–410 (1994)

Beyn, W., Champneys, A., Doedel, E., Govaerts, W., Kuznetsov, Y.A., Sandstede, B.: Numerical Continuation, and Computation of Normal Forms. Handbook of Dynamical Systems, pp. 149–219. North-Holland, Amsterdam (2002)
Broer, H.W., Chow, S.-N., Kim, Y.-I., Vegter, G.: The Hamiltonian double-zero eigenvalue. In: Normal forms and homoclinic chaos (Waterloo, ON, 1992), volume 4 of Fields Institute Communication, pp. 1–19. American Mathematical Society, Providence, RI (1995)
Buono, P.L., Montaldi, J., Laurent-Polz, F.: Symmetric hamiltonian bifurcations. In: Montaldi, J., Ratiu, T. (eds.) Geometric Mechanics and Symmetry : The Peyresq Lectures, London Mathematical Society Lecture Note Series, pp. 357–402. Cambridge University Press, Cambridge (2005)
Burgos-García, J., Lessard, J.P., James, J.D.M.: Spatial periodic orbits in the equaliteral circular restricted four body problem: computer assisted proofs of existence. (Submitted), (2018)
Burgos-García, J.: Families of periodic orbits in the planar Hill's four-body problem. Astrophys. Space Sci. **361**(11), 21 (2016)
Burgos-Garcia, J., Bengochea, A.: Horseshoe orbits in the restricted four-body problem. Astrophys. Space Sci. **362**(11), 14 (2017)
Burgos-García, J., Delgado, J.: On the "blue sky catastrophe" termination in the restricted four-body problem. Celest. Mech. Dynam. Astronom. **117**(2), 113–136 (2013)
Burgos-García, J., Delgado, J.: Periodic orbits in the restricted four-body problem with two equal masses. Astrophys. Space Sci. **345**(2), 247–263 (2013)
Burgos-García, J., Gidea, M.: Hill's approximation in a restricted four-body problem. Celest. Mech. Dynam. Astronom. **122**(2), 117–141 (2015)
Cabré, X., Fontich, E., de la Llave, R.: The parameterization method for invariant manifolds. I. Manifolds associated to non-resonant subspaces. Indiana Univ. Math. J. **52**(2), 283–328 (2003)
Cabré, X., Fontich, E., de la Llave, R.: The parameterization method for invariant manifolds. II. Regularity with respect to parameters. Indiana Univ. Math. J. **52**(2), 329–360 (2003)
Cabré, X., Fontich, E., de la Llave, R.: The parameterization method for invariant manifolds. III. Overview and applications. J. Differ. Equ. **218**(2), 444–515 (2005)
Calleja, R.C., Doedel, E.J., Humphries, A.R., Lemus-Rodríguez, A., Oldeman, E.B.: Boundary-value problem formulations for computing invariant manifolds and connecting orbits in the circular restricted three body problem. Celest. Mech. Dyn. Astronom. **114**(1–2), 77–106 (2012)
Canalias, E., Delshams, A., Masdemont, J.J., Roldán, P.: The scattering map in the planar restricted three body problem. Celest. Mech. Dyn. Astronom. **95**(1–4), 155–171 (2006)
Capiński, M., Roldán, P.: Existence of a center manifold in a practical domain around L_1 in the restricted three body problem. SIAM J. Appl. Dyn. Syst. **11**(1), 285–318 (2011)
Champneys, A.R.: Homoclinic orbits in reversible systems and their applications in mechanics, fluids and optics. volume 112, pages 158–186. (1998). Time-reversal symmetry in dynamical systems (Coventry, 1996)
Champneys, A.R., Kuznetsov, Y.A.: Numerical detection and continuation of codimension-two homoclinic bifurcations. Int. J. Bifur. Chaos Appl. Sci. Engrg. **4**(4), 785–822 (1994)
Champneys, A.R., Toland, J.F.: Bifurcation of a plethora of multi-modal homoclinic orbits for autonomous Hamiltonian systems. Nonlinearity **6**(5), 665–721 (1993)
Champneys, A.R., Härterich, J., Sandstede, B.: A non-transverse homoclinic orbit to a saddle-node equilibrium. Ergodic Theory Dyn. Syst. **16**(3), 431–450 (1996)
Champneys, A.R., Kuznetsov, Y.A., Sandstede, B.: A numerical toolbox for homoclinic bifurcation analysis. Int. J. Bifur. Chaos Appl. Sci. Engrg. **6**(5), 867–887 (1996)
Cheng, X., She, Z.: Study on chaotic behavior of the restricted four-body problem with an equilateral triangle configuration. Int. J. Bifur. Chaos Appl. Sci. Engrg. **27**(2), 1750026 (2017)
Chicone, C.: Ordinary Differential Equations with Applications, Volume 34 of Texts in Applied Mathematics, 2nd edn. Springer, New York (2006)
Cobos, J., Simó, C.: Reduction of the central manifold around a collinear equilibrium point of the restricted three-body problem. In: XV Congress on Differential Equations and Applications/V Congress on Applied Mathematics, Vol. I, II (Spanish) (Vigo, 1997), volume 9 of Colecc. Congress, pp. 673–676. University of Vigo Services Publication, Vigo (1998)
Deng, B.: Homoclinic bifurcations with nonhyperbolic equilibria. SIAM J. Math. Anal. **21**(3), 693–720 (1990)
Devaney, R.L.: Homoclinic orbits in Hamiltonian systems. J. Differ. Equ. **21**(2), 431–438 (1976)
Devaney, R.L.: Blue sky catastrophes in reversible and Hamiltonian systems. Indiana Univ. Math. J. **26**(2), 247–263 (1977)
Dhooge, A., Govaerts, W., Kuznetsov, Y.A., Mestrom, A., Riet, A.M., Sautois, B.: MatCont and CLMatCont: Continuation Toolbox in MATLAB, (2006)

Doedel, E.J., Friedman, M.J.: Numerical computation of heteroclinic orbits. J. Comput. Appl. Math. **26**(1–2), 155–170 (1989). Continuation techniques and bifurcation problems

Doedel, E.J., Friedman, M.J., Kunin, B.I.: Successive continuation for locating connecting orbits. Numer. Algorithms **14**(1–3), 103–124 (1997). Dynamical numerical analysis (Atlanta, GA, 1995)

Doedel, E.J., Paffenroth, R.C., Keller, H.B., Dichmann, D.J., Galán-Vioque, J., Vanderbauwhede, A.: Computation of periodic solutions of conservative systems with application to the 3-body problem. Int. J. Bifur. Chaos Appl. Sci. Engrg. **13**(6), 1353–1381 (2003)

Farrés, A., Jorba, À.: On the high order approximation of the centre manifold for ODEs. Discrete Contin. Dyn. Syst. Ser. B **14**(3), 977–1000 (2010)

Friedman, M.J., Doedel, E.J.: Computational methods for global analysis of homoclinic and heteroclinic orbits: a case study. J. Dyn. Differ. Equ. **5**(1), 37–57 (1993)

Gameiro, M., Lessard, J.-P., Pugliese, A.: Computation of smooth manifolds via rigorous multi-parameter continuation in infinite dimensions. Found. Comput. Math. **16**(2), 531–575 (2016)

Gidea, M., Burgos, M.: Chaotic transfers in three- and four-body systems. Phys. A **328**(3–4), 360–366 (2003)

Gómez, G., Jorba, À., Simó, C., Masdemont, J.: Dynamics and mission design near libration points. Vol. III, volume 4 of World Scientific Monograph Series in Mathematics. World Scientific Publishing Co., Inc., River Edge, NJ, (2001). Advanced methods for collinear points

Gómez, G., Jorba, À., Simó, C., Masdemont, J.: Dynamics and mission design near libration points. Vol. IV, volume 5 of World Scientific Monograph Series in Mathematics. World Scientific Publishing Co., Inc., River Edge, NJ, (2001). Advanced methods for triangular points

Gómez, G., Llibre, J., Martínez, R., Simó, C.: Dynamics and mission design near libration points. Vol. I, volume 2 of World Scientific Monograph Series in Mathematics. World Scientific Publishing Co., Inc., River Edge, NJ, (2001). Fundamentals: the case of collinear libration points, With a foreword by Walter Flury

Gómez, G., Simó, C., Llibre, J., Martínez, R.: Dynamics and mission design near libration points. Vol. II, volume 3 of World Scientific Monograph Series in Mathematics. World Scientific Publishing Co., Inc., River Edge, NJ, (2001). Fundamentals: the case of triangular libration points

Haro, À., Canadell, M., Figueras, J.-L., Luque, A., Mondelo, J.-M.: The Parameterization Method for Invariant Manifolds, Volume 195 of Applied Mathematical Sciences. Springer, Cham (2016). From rigorous results to effective computations

Henrard, J.: Proof of a conjecture of E. Strömgren. Celest. Mech. **7**, 449–457 (1973)

Homburg, A.J., Knobloch, J.: Bellows bifurcating from degenerate homoclinic orbits in conservative systems. In: EQUADIFF 2003, pp. 963–971. World Science Publication, Hackensack, NJ (2005)

Iooss, G., Kirchgässner, K.: Water waves for small surface tension: an approach via normal form. Proc. R. Soc. Edinburgh Sect. A **122**(3–4), 267–299 (1992)

James, J.D.M.: Polynomial approximation of one parameter families of (un)stable manifolds with rigorous computer assisted error bounds. Indag. Math. **26**(1), 225–265 (2015)

Jorba, À., de la Llave, R., Zou, M.: Lindstedt series for lower-dimensional tori. In: Hamiltonian systems with three or more degrees of freedom (S'Agaró, 1995), volume 533 of NATO Advances Science Institute Series C Mathematical Physics Science, pp. 151–167. Kluwer Acadamic Publication, Dordrecht (1999)

Jorba, À.: A methodology for the numerical computation of normal forms, centre manifolds and first integrals of Hamiltonian systems. Exp. Math. **8**(2), 155–195 (1999)

Jorba, À., Masdemont, J.: Dynamics in the center manifold of the collinear points of the restricted three body problem. Phys. D **132**(1–2), 189–213 (1999)

Jorba, À., Villanueva, J.: Numerical computation of normal forms around some periodic orbits of the restricted three-body problem. Phys. D **114**(3–4), 197–229 (1998)

Kepley, S., James, J.D.M.: Homoclinic dynamics in a restricted four-body problem: transverse connections for the saddle-focus equilibrium solution set. Celest. Mech. Dynam. Astronom. **131**(3), 55 (2019)

Kepley, S., James, J.D.M.: Chaotic motions in the restricted four body problem via Devaney's saddle-focus homoclinic tangle theorem. J. Differ. Equ. **266**(4), 1709–1755 (2019)

Knobloch, J.: Bifurcation of degenerate homoclinic orbits in reversible and conservative systems. J. Dyn. Differ. Equ. **9**(3), 427–444 (1997)

Kokubu, H.: Homoclinic and heteroclinic bifurcations of vector fields. Jpn. J. Appl. Math. **5**(3), 455–501 (1988)

Kuznetsov, Y.A.: Elements of Applied Bifurcation Theory, Volume 112 of Applied Mathematical Sciences, 3rd edn. Springer, New York (2004)

Kuznetsov, Y.A., Meijer, H.G.E.: Numerical Bifurcation Analysis of Maps, Volume 34 of Cambridge Monographs on Applied and Computational Mathematics. Cambridge University Press, Cambridge (2019). From theory to software

Leandro, E.S.G.: On the central configurations of the planar restricted four-body problem. J. Differ. Equ. **226**(1), 323–351 (2006)
Meyer, K.R., Offin, D.C.: Introduction to Hamiltonian dynamical systems and the N-body problem, Volume 90 of Applied Mathematical Sciences, 3rd edn. Springer, Cham (2017)
Muñoz Almaraz, F.J., Freire, E., Galán, J., Doedel, E., Vanderbauwhede, A.: Continuation of periodic orbits in conservative and Hamiltonian systems. Phys. D **181**(1–2), 1–38 (2003)
Murray, M., James, J.D.M.: Chebyshev-taylor parameterization of stable/unstable manifolds for periodic orbits: implementation and applications. Int. J. Bifur. Chaos Appl. **27**(14), 1730050 (2017)
Murray, M., James, J.D.M.: Homoclinic dynamics in a spatial restricted four-body problem: blue skies into Smale horseshoes for vertical Lyapunov families. Celest. Mech. Dynam. Astronom. **132**(6–7), 44 (2020)
Oldeman, B.E., Krauskopf, B., Champneys, A.R.: Numerical unfoldings of codimension-three resonant homoclinic flip bifurcations. Nonlinearity **14**(3), 597–621 (2001)
Oldeman, B.E., Champneys, A.R., Krauskopf, B.: Homoclinic branch switching: a numerical implementation of Lin's method. Int. J. Bifur. Chaos Appl. Sci. Engrg. **13**(10), 2977–2999 (2003)
Papadakis, K.E.: Families of asymmetric periodic solutions in the restricted four-body problem. Astrophys. Space Sci. **361**(12), 377 (2016)
Papadakis, K.E.: Families of three-dimensional periodic solutions in the circular restricted four-body problem. Astrophys. Space Sci. **361**(4), 14 (2016)
Pedersen, P.: Librationspunkte im restringierten vierkörperproblem. Dan. Mat. Fys. Medd. **21**(6), 1–80 (1944)
Pedersen, P.: Stabilitätsuntersuchungen im restringierten vierkörperproblem. Dan. Mat. Fys. Medd. **26**(16), 1–38 (1952)
She, Z., Cheng, X.: The existence of a Smale horseshoe in a planar circular restricted four-body problem. Celest. Mech. Dynam. Astronom. **118**(2), 115–127 (2014)
She, Z., Cheng, X., Li, C.: The existence of transversal homoclinic orbits in a planar circular restricted four-body problem. Celest. Mech. Dynam. Astronom. **115**(3), 299–309 (2013)
Shilnikov, L.P., Shilnikov, A.L., Turaev, D.V.: Showcase of blue sky catastrophes. Int. J. Bifur. Chaos Appl. Sci. Engrg. **24**(8), 1440003 (2014)
Simó, C.: Estimates of the error in normal forms of Hamiltonian systems. Applications to effective stability and examples. In: Long-term dynamical behaviour of natural and artificial N-body systems (Cortina d'Ampezzo, 1987), volume 246 of NATO Advanced Science Institutes Series C Mathematical Physics Science, pp. 481–503. Kluwer Academic Publication, Dordrecht, (1988)
Simo, C.: On the Analytical and Numerical Approximation of Invariant Manifolds. In: Benest, D., Froeschle, C. (eds.), Modern Methods in Celestial Mechanics, Comptes Rendus de la 13ieme Ecole Printemps d'Astrophysique de Goutelas (France), 24–29 Avril, 1989. Edited by Daniel Benest and Claude Froeschle. Gif-sur-Yvette: Editions Frontieres, 1990., p. 285, page 285, (1990)
Simó, C.: Relative equilibrium solutions in the four-body problem. Celest. Mech. **18**(2), 165–184 (1978)
Strömgren, E.: Connaissance actuelle des orbites dans le probleme des trois corps. Bull. Astron. **9**, 87–130 (1934)
Szebehely, V.: Theory of Orbits. Academic Press Inc., Cambridge (1967)
van den Berg, J.B., Hetebrij, W., Rink, B.: More on the parameterization method for center manifolds. (Submitted), (2020)
van den Berg, J.B., Breden, M., Lessard, J.-P., Murray, M.: Continuation of homoclinic orbits in the suspension bridge equation: a computer-assisted proof. J. Differ. Equ. **264**(5), 3086–3130 (2018)
Weihua, D., Huang, M.: On homoclinic bifurcation emanating from Takens-Bogdanov points in Hamiltonian systems. Z. Angew. Math. Phys. **54**(2), 256–272 (2003)